Divalent metal release and antimicrobial effects of layered double hydroxides

Jazia Awassa, Damien Cornu, Samantha Soulé, Cédric Carteret, Christian Ruby, Sofiane El-Kirat-Chatel

Divalent Metal Release and Antimicrobial Effects of Layered Double Hydroxides

Jazia Awassa[1], Damien Cornu[1], Samantha Soulé[1], Cédric Carteret[1],

Christian Ruby[1]*, Sofiane El-Kirat-Chatel[1]

[1]Laboratoire de Chimie Physique et Microbiologie pour les Matériaux et l'Environnement (LCPME), Université de Lorraine, 405 Rue de Vandoeuvre, 54600, Villers-lès-Nancy, France

*Corresponding author:

Christian Ruby: Christian.ruby@univ-lorraine.fr

Abstract

Resistance to antimicrobial agents is responsible for major social and economic losses. The World Health Organization estimated 700,000 global deaths a year due to antimicrobial resistance. The use of layered double hydroxides (LDHs) as antibacterial materials could present a way to reduce the risk of bacterial infections and antibacterial resistance, by partial release of metallic ions in aqueous dispersion. The partial dissolution of different synthetic LDHs M^{II}-Al^{III} (M= Zn, Cu, Ni, Co, Mg) was studied in Lysogeny Broth (LB) and Tryptic Soy Broth (TSB), growth media of *Escherichia coli (E. coli)* and *Staphylococcus aureus (S. aureus)* bacteria, respectively. The influence of several parameters (crystallinity, M^{II}:Al^{III} ratio, type of intercalated anion {CO_3^{2-}, Cl^-, NO_3^-, ClO_4^-} and nature of M^{II} cations) was investigated. In the absence of any post-synthetic hydrothermal treatment, Zn^{II}-Al^{III} LDH showed a release of Zn^{II} ions 6 times enhanced. Upon increasing Zn^{II}:Al^{III} molar ratio to 3 : 1 and exchanging carbonate anions with other anions having lower intercalating affinities, a similar effect was observed . The dissolution properties of M^{II}-Al^{III} LDHs were correlated with the thermodynamic stability of their $M^{II}(OH)_2$ hydroxide counterparts with the exception of Cu^{II}-based LDH, which showed an amplified release of Cu^{II} due to its irregular structure presenting defects. Finally, the antibacterial activity was only noted for Zn^{II} and Cu^{II}-based LDHs. The antimicrobial effect of the studied LDHs was linked in the first place to the nature of divalent metal itself, and to the amount of released M^{II} ions into the culture media in the second place. This effect was more easily identified in Zn^{II}-Al^{III} LDHs whose minimum inhibitory concentration was decreased significantly from 12 to 0.375 $mg.mL^{-1}$ when higher amounts of Zn^{II} ions were released.

Keywords

LDHs

Dissolution

Bacterial inhibition

Crystallinity

Zinc

Copper

1. Introduction

Layered double hydroxides (LDHs) are clay lamellar solids having a structure based on the stacking of brucite-like sheets compromising divalent and trivalent metal hydroxides. These sheets hold a net positive charge which is compensated by negatively charged intercalating anions and water molecules present in the interlaminar regions. The general formula of LDH can be expressed as: $[M(II)_{(1-x)}\ M(III)_x\ (OH)_2]^{x+}\ [A^{n-}_{x/n}\ .\ yH_2O]^{x-}$, where M(II) and M(III) are divalent and trivalent metal cations, respectively, and A^{n-} is an n-valent intercalating anion **(Bini & Monteforte, 2018; Rives, 2001; Theiss et al., 2016)**. Due to their interesting properties, including anion exchangeability, compositional flexibility, and biocompatibility, LDHs have found themselves various technological applications such as catalysis **(Yang et al., 2021)**, sorption of pollutants **(Johnston et al., 2021)**, bio-sensors **(Inmauddin, 2019)**, drug storage delivery **(Bi et al., 2014)**, photocatalytic water remediation **(L. Wang et al., 2021)** and antimicrobial materials **(León-Vallejo et al., 2019; Mishra et al., 2018)**.

Nowadays, the fabrication of different materials avoiding biofouling or pathogenic bacteria proliferation is highly demanded **(Forano et al., 2018)**. Under this aspect, LDH and LDH-composite materials were utilized in different antimicrobial applicational fields as water purification **(Kamal et al., 2018; Moaty et al., 2016)**, food packaging **(Cheng et al., 2019; Tammaro et al., 2014)**, wound healing dressings **(W. Zhang et al., 2020),** and textile industries **(Mallakpour et al., 2021).** In fact, many surveys showed that LDHs possess high potential as carriers of biological antibiotics due to their controlled release rate **(Djebbi et al., 2016; Salguero et al., 2020; Y. Wang & Zhang, 2012)**. Antibiotics can treat bacterial infections, however, the excessive use of antibiotic had led to emergence of new antimicrobials and spread

of resistant strains **(El-Shahawy et al., 2018; Williams et al., 2019)**, where the World Health Organization (WHO) estimates 700,000 global deaths per year due to antimicrobial resistance phenomenon **(WHO, 2019)**. Moreover, some work had been reported on the loading of antimicrobial metallic nanoparticles as silver nanoparticles within the LDH matrix to achieve an efficient antimicrobial effect **(Mao et al., 2019; Marcato et al., 2013; Mishra et al., 2013)**. Although these metallic nanoparticles-LDH composites exhibit significant antibacterial effects, the toxicity caused by their aggregation behavior is still the main challenge in such applications **(Bélteky et al., 2019; Carja et al., 2009; Sharma & Prasher, 2020)**.

On the other hand, some recent studies proved that unmodified pristine LDHs could also act as efficient antibiotic-free antimicrobial materials where Moaty *et al.* showed that pristine Zn^{II}-Fe^{III} possess a durable antimicrobial activity against several Gram-positive and Gram-negative bacteria **(Moaty et al., 2016)**. Peng *et al.* compared the antimicrobial properties of Mg^{II}-based LDHs to those of Zn^{II}-based ones and found out that the latter showed better antibacterial properties **(Peng et al., 2018)**. Dutta *et al.* also reported contribution of Zn^{II}-based LDH to an efficient antimicrobial effect **(Dutta et al., 2020)**. Moreover, Sanchez *et al.* found out that the antibacterial activity of pristine Zn^{II}-Al^{III} LDHs could be enhanced by increasing the Zn^{II}-Al^{III} molar ratio **(Lobo-Sánchez et al., 2018)**. Another recent study also highlighted the superior antimicrobial effect of Zn^{II}-based LDHs in comparison to Mg^{II} and Cu^{II}-based LDHs against *Corynebacterium ammoniagenes* (*C. ammoniagene*) **(León-Vallejo et al., 2019).** The antimicrobial properties of Cu^{II}-substituted Zn^{II}-Al^{III} and its calcined products was also investigated, where calcined LDHs at higher temperatures performed better in antibacterial tests due to their smaller particle sizes promoting better contact **(Mishra et al., 2018)**. Similarly,

Tabti *et al.* was able to prove the antimicrobial activity of ternary MgCuAl LDHs which was primary dependent on the Cu^{II}:Al^{III} molar ratio in the LDHs **(Tabti et al., 2020).**

Despite the fact that several hypotheses were proposed by these studies to explain the antimicrobial effect of pristine LDHs or their derived metal oxides counterparts, the followed antibacterial mechanism is still not well understood. The partial dissolution of pristine LDHs into their constituents M^{II} aqueous ions might constitute one possible mechanism explaining their antibacterial activities **(León-Vallejo et al., 2019; Li et al., 2019; Peng et al., 2018; Rocha Oliveira et al., 2015)**. Although such antimicrobial mode of action was suggested**,** no real experimental set up was designed to validate it and no proof of experimental evidence was reported up until now. Moreover, these studies do not provide systematic approaches to determine in depth how to tune the physicochemical parameters of pristine LDHs to enhance the desired antimicrobial effect. Indeed, Vallejo *et al.* linked the antimicrobial effect of Zn^{II} and Cu^{II}-based LDHs to the amount of present cations in the powders, but not to the amount of released cations in the microbial culture media **(León-Vallejo et al., 2019)**. Rasouli *et al.* related the antibacterial efficiency of mixed metal oxide nanoparticles derived from Zn^{II}-Al^{III} LDHs directly to their crystallite sizes which may affect the solubility of the LDHs **(Rasouli et al., 2017)**. An insight concerning the role of released soluble zinc species on the toxicity of zinc oxide (ZnO) nanoparticles was established in some previous work **(Esteban-Tejeda et al., 2017; M. Li et al., 2011)**. However, these studies do not study systematically all parameters leading to the dissolution of the powders. Moreover, oxides have different compositional and physicochemical properties than those of LDHs, and would thus perform differently in terms of dissolution and antimicrobial effect. Under such circumstances, the study of the different parameters influencing the release behavior of Zn^{II} in aqueous bacterial growth broth media, or any other metallic cation

possessing an antimicrobial activity out of LDHs is of upmost importance for evaluating and understanding such antimicrobial effect.

The exposure of LDH powders to aqueous solutions in which dissolution can certainly take place may play an important role in their several potential applications including antimicrobial ones. However, the subject had been unattended by the literature and the available evidences are scarce. In fact, some early studies evaluated the stability and dissolution properties of layered double hydroxides using thermodynamical approaches **(Allada, 2002; Allada et al., 2005; Boclair & Braterman, 1999)**. Such approaches are very interesting but also based on computational investigations, thus lacking real measurements in solution.

In 2011, Jobbagy *et al.* studied the release behavior of metallic ions from a synthetic chloride-containing MgAl LDH at a pH range of 1-9, in order evaluate its chemical stability and to assess the operating dissolution mechanisms **(Jobbágy & Regazzoni, 2011)**. Another study mainly focused on the investigation of the cytotoxicity of hydrotalcites bearing different intercalated anions by evaluating the average dissolution profiles of Mg^{II} from MgAl-CO_3 and MgAl-Cl in both simulated body and lysosomal fluids **(Baek et al., 2011)**. The stability of these LDHs varied in accordance to the nature of intercalated anion, which also affected their cytotoxicity behavior. Moreover, Hibino reported the effect of crystallinity of carbonate-intercalated Mg-Al LDHs on their dissolution and anion exchange properties in different aqueous acetate buffer/NaCl media having a pH of 5.3 **(Hibino, 2014)**. Compared to higher crystallinity LDHs, lower crystallinity ones showed lower extent of exchange of interlayer anions and greater weight loss of M^{II}:Al^{III} implying greater release of M^{II} in aqueous media. Although these investigations considered real measurements of dissolved species in aqueous solutions, nonetheless, they were not devoted to

study in a systematic way the dissolution properties of LDHs. In other words, only the influence of one or a limited number of parameters on the dissolution properties of LDHs was considered, where in fact several factors may contribute to LDH dissolution, *e.g.*, crystallinity, nature of constituent metallic cations and M^{II}:Al^{III} molar ratio, as well as the type of intercalated anions within the layers. Thus, a global investigation concerning the different factors affecting the solubility of LDHs seems to be of great importance in this area.

In this context, the present study aims to evaluate systematically the influence of different parameters (crystallinity, M^{II}:Al^{III} ratio, type of intercalated anion {CO_3^{2-}, Cl^-, NO_3^-, ClO_4^-} and nature of M^{II} cations) on the solubility of pristine LDHs in broth media thus leading to their antimicrobial effect. The properties of Zn^{II}-based LDHs had been systematically analyzed due to their relatively well-established antimicrobial behavior. The dissolution properties of the prepared M^{II}-Al^{III} LDHs were studied in growth media of *Escherichia coli* and *Staphylococcus aureus* bacteria, *i.e.* Lysogeny Broth (LB) and Tryptic Soy Broth (TSB), respectively. Finally, the relationship between the solubility and physicochemical properties of the LDHs and their antimicrobial activity was determined and subsequently the antimicrobial mechanism of pristine LDHs by metallic ions release was validated.

2. Experimental section

2.1.Materials

Aluminum nitrate nonahydrate ($Al(NO_3)_3.6H2O$, ≥99 %), Zinc nitrate hexahydrate ($Zn(NO3)_2.6H2O$, ≥ 99 %, Copper (II) nitrate trihydrate ($Cu(NO_3)_2.3H_2O$, ≥99%), Nickel (II) nitrate hexahydrate ($Ni(NO_3)_2.6H_2O$, ≥99%), Cobalt (II) nitrate hexahydrate ($Co(NO_3)_2.6H_2O$, ≥98%), Magnesium nitrate hexahydrate ($Mg(NO_3)_2.6H_2O$, ≥99%), Sodium carbonate (Na_2CO_3),

Hydrochloric acid (HCl, 37%), Nitric acid (HNO_3, 65%) Luria Bertani Broth (LB), Tryptic Soy Broth (TSB), Agar-agar, Phosphate Buffered Saline (PBS) tablets were purchased from SIGMA-ALDRICH. Ammonia solution (S.G. 0.88, 35%) was purchased from Fisher Scientific. Sodium hydroxide solution (1 $mol.L^{-1}$) and Perchloric acid ($HClO_4$, 60%) were purchased from VWR Chemicals and Raedel-de Haen, respectively. Antibiotic filter discs (6mm) and sterile cotton tipped swabs were purchased from Dominique Dutscher and COPAN, respectively. The standards used for ICP-MS tests were prepared in the laboratory from commercial solutions certified at 1000 ppm (Merck).

2.2. Synthesis of carbonate intercalated layered double hydroxides

Carbonate intercalated LDHs marked as $M_2Al:CO_3$ (M= Zn, Cu, Ni, Co, Mg) and $M_3Al:CO_3$ (M= Zn) were synthesized by a simple coprecipitation method **(Kim et al., 2017)**. First a 0.05 M ammonium/ammonia solution was prepared then the pH of the solution was fixed to a value of 10 using a solution of 1% HNO_3. A solution of 0.4 $mol.L^{-1}$ M^{II} and Al^{III} nitrate salts having a molar ratio M^{II}:Al^{III} of 2:1 or 3:1 was added slowly using a peristaltic pump operated at 0.3 $mL.min^{-1}$ into the ammonia solution. The pH was kept constant at 10 by an automatic titrator (736 GP Titrino, Metrohm) using a solution of 1 $mol.L^{-1}$ NaOH and 0.25 $mol.L^{-1}$ Na_2CO_3. For most of the synthesis, this was followed by a hydrothermal treatment in an autoclave at 80°C for 24 hours to enhance the crystallinity, then the solids were washed for 4 times in deionized water and collected by centrifugation at 10000 rpm. Finally, the obtained LDH solids were dried in air at 80°C for 24 hours. Only one LDH, denoted as *$Zn_2Al:CO_3$-cop*, was not exposed to hydrothermal treatment, where the solid obtained directly after coprecipitation was washed and dried without any further treatment. The detailed experimental conditions for the synthesis of

carbonate intercalated LDHs are provided in **Table S1. (See supplementary material)** The synthesized LDHs were denoted as $M_xAl:A^{n-}$, where M is the constituent divalent metal of the LDH, Al corresponds to the constituent trivalent aluminum metal, x is the molar ratio of divalent to trivalent metal ($M^{II}:Al^{III}$) and A^{n-} is the intercalated anion in the interlayer space.

2.3. Synthesis of chloride, nitrate and perchlorate intercalated Zn_2Al layered double hydroxides

$Zn_2Al:Cl$, $Zn_2Al:NO_3$ and $Zn_2Al:ClO_4$ LDHs were prepared by anion exchange reaction of $Zn_2Al:CO_3$-hyd in presence of acid-alcohol mixed solutions following the method adapted by Iyi *et al.* **(Iyi et al., 2011)**. Briefly, 1 mmol of $Zn_2Al:CO_3$ was dispersed in 30 mL ethanol, then 1.986 mmol of strong acid (HCl, HNO_3, $HClO_4$) present in 20 mL of ethanol solution was added, to avoid brutal contact between the solid and the acid thus limiting the dissolution of the LDHs. The whole exchange process was allowed to take place at 50°C for 1 hour under vigorous stirring and nitrogen (N_2) flow to promote a total exchange. The samples were then filtered on a Buchner funnel, washed with distilled water and finally dried in air at 80°C.

2.4.Characterization

$M^{II}:Al^{III}$ molar ratios of LDHs were measured by Induced Couple Plasma Mass Spectroscopy (ICP-MS Agilent-7800). 10 mg of LDH were dissolved into 1% HNO_3. The calibration range was set as 10 to 3000 ppb. The detected isotopes were: ^{27}Al, ^{66}Zn, ^{63}Cu, ^{60}Ni, ^{59}Co, ^{26}Mg.

Powder X-Ray Diffraction (PXRD) characterization at room temperature of the obtained powders was performed using a Panalytical X'Pert Pro MPD diffractometer in reflection geometry using Cu radiation ($K\alpha_1$ = 1.5406 Å), a Ge(111) incident-beam monochromator, Soller slits of 0.02 rad, programmable divergence and anti-scatter slits. The irradiated area was fixed to

10mm x 10mm, and an X'Celerator detector was used. Data were collected from finely ground samples with a sample holder spinner and continuous rotation of sample to improve statistical representation of the samples. All the powder diffraction data were collected using the same procedure, *i.e.* at the same scattering angle range (between 5 and 70°) with a 0.0167°step and a speed of 1°/min. Lattice parameters were extracted from cell refinements of the LDH phases. The average crystallite size, calculated as XRD coherent domains, in the directions perpendicular ($L_{(003)}$) and parallel ($L_{(110)}$) to the hydroxide layers of the obtained LDHs were estimated from the full width at half maximum (FWHM) values of the respective diffraction reflections (003) and (110) using the Scherrer equation Erreur ! Source du renvoi introuvable.**)**:

$$\boldsymbol{L = \frac{K\,\lambda}{\beta\,cos\theta}} \qquad \textbf{(1)}$$

Where *K* is the Scherrer constant (0.9), λ is incident ray wavelength, β is the full width at half maximum in radians, and θ is the Bragg angle (rad) **(Cullity, 1978)**.

Raman spectroscopy characterizations were performed using a confocal Raman microscope (inVia® Qontor with a Peltier-cooled charge-coupled device (CCD) camera, Renishaw, Wotton-under-Edge, UK) equipped with a 532 nm laser, a 50x objective with 0.55 of numerical aperture, and a 2400 lines.mm^{-1} grating. The spectral resolution was about 3 cm^{-1} (10 acquisitions of 5 seconds). Each sample was analyzed at different points to check the uniformity of the studied hydroxides. The laser power was changed in the range of 50 to 1 mW depending on the type of LDH sample and the spectra were recorded in the 400 to 4000 cm^{-1} wavenumber range.

Infrared spectra were recorded in the mid-infrared range on a Bruker Vertex 70v spectrometer equipped with a KBr beam-splitter and a deuterated triglycine sulfate (DTGS) detector. An attenuated total reflection (ATR) accessory (Platinum ATR with a single reflection diamond

crystal, Bruker) was used for acquiring spectra of the LDH powders. The spectral resolution was 4 cm^{-1} and the accumulation time was 1 min (100 scans). Compartments containing the detector and the ATR accessory were under vacuum (<1 hPa).

Specific surface area analysis of Zn^{II}-Al^{II} LDH samples were performed using the Brunauer-Emmet-Teller (BET) approach using a BELSORP MAX analyzer at 77K in N_2. The powders were degassed at 120°C prior to the measurements to remove any adsorbed water molecules.

Particle size distribution (PSD) of Zn^{II}-Al^{II} LDH samples was determined by Laser Diffraction using a Diffraction Mastersizer 3000 equipment from Malvern Instruments. 50 mg of dry powder was dispersed in 100 mL water using dispersion unit Hydro 2000 also from Malvern Instruments. Control tests were done in LB and TSB media for one LDH sample, and the PSD of this sample was the same as that done in distilled water, thus all other tests were conducted in distilled water for easier manipulation, time and economy saving. Three consecutive PSD measurements were carried out with a time interval separation of 2 minutes, in order to determine the volume median diameter (D_{v50}) and the surface area mean diameter ($D_{[3, 2]}$) for each sample.

The morphology of some LDH samples was examined by Scanning Electron Microscopy (SEM) performed on a JEOL JSM-IT500HR, with a Field Emission Gun (FEG) and a voltage of analysis situated in between 2kV and 5 kV. The analysis was performed under high vacuum, and 60µm diaphragm aperture was settled. Secondary Electron Detector (SED) was used for imaging.

2.5.Partial dissolution experiments

Partial dissolution profiles of the prepared LDHs into their constituents divalent and trivalent metal was measured by dispersing 10 $mg.mL^{-1}$ of LDHs in both Lysogeny Broth (LB) and

Tryptic Soy Broth (TSB). After a given incubation time of 48 hours at 37°C, the supernatants were collected by centrifugation. Finally, the metal concentration in the supernatant was measured by Induced Couple Plasma Mass Spectroscopy (ICP-MS Agilent-7800). Control partial dissolution experiments were also done in Milli-Q water under the same experimental conditions. Each experiment was repeated at least 3 times and the average dissolution of metals out of LDH powders was determined. The kinetic release profiles of Zn^{II} from Zn_2AlCO_3-hyd and Zn_2AlCO_3-cop was studied in LB, TSB using the same mass concentration over 48 hours as well.

2.6. Antibacterial experiments

2.6.1. Agar disc diffusion test

The anti-bacterial activity of the synthesized LDHs was evaluated against two different pathogenic bacteria: *E. coli* (Gram-negative) and *S. aureus* (Gram-positive) using agar disc diffusion assay. All experiments were repeated three times to ensure their reproducibility. First, *E. coli* and *S. aureus* were precultured overnight in 5 mL of LB and TSB respectively. LB and TSB agar plates were prepared, sterilized and solidified. Then, 250 µL of bacterial suspension were diluted to 1/1500 in sterile PBS and spread on LB and TSB agar plates using a sterile cotton swab to prepare bacterial lawns monolayers. Antibiotic filter discs of 6 mm were placed on these plates and 20 µL of LDH dispersions (10 $mg.mL^{-1}$) were loaded on the respective discs. The plates were then incubated at 37°C for 48 h. Afterwards, bacterial inhibition zones were observed around the discs. The diameter of the circular zones was measured using a centimeter ruler and mean values of three repeated trials for each microorganism were recorded and represented in millimeters. A similar procedure was followed to investigate the antimicrobial activity of

metallic salts counterparts having a molar concentration of 3 mmol.L^{-1} for Zn^{II}, Ni^{II}, Co^{II} and Mg^{II} salts (the average released concentration of metallic cations out of their LDH samples counterparts) and 10 mmol.L^{-1} for Cu^{II} salts (the average released concentration of Cu^{II} out of $Cu_2Al{:}CO_3$ LDH sample). Each test was repeated three times to ensure the reproducibility of our experiments and the mean inhibition diameter was calculated.

2.6.2. Turbidimetric method for MIC determination

Broth microdilution turbidimetric method was used to determine the minimum inhibitory concentration (MIC) of the prepared Zn^{II}-based LDH powders. *E. coli* and *S. aureus* were precultured in 5 mL of LB and TSB, respectively. An inoculum of each of strain was prepared and diluted to obtain an optical density of 0.1 at λ = 600 nm (OD_{600}=0.1). Zn^{II}-based LDH powders were dispersed in broth culture media (LB or TSB), and two-fold dilution series were then prepared in a 96-well Micro-titer plate. Each well included 25 µL of the diluted LDH powder and 175 µL of bacterial inoculum. Un-inoculated broth wells containing the different used LDH dispersion concentrations were used as a negative standard growth control. As a positive control, 12 wells were prepared with 175 µL of bacterial inoculum and 25 µL of broth culture media. The Micro-titer plate was then sealed and incubated at 37°C under agitation for 48 hours. The MIC value for each LDH sample was recognized as the lowest concentration that had no visible turbidity. Experiments were repeated at least 2 times for each sample and the wells corresponding to the obtained MIC values were the same.

3. Results and discussion

3.1. Characterization of the LDHs

3.1.1. Structural features: M^{II}:Al^{III} molar ratio determination, Powder X-Ray Diffraction, Infra-Red and Raman spectroscopies analysis

Carbonate-intercalated LDHs were synthesized by coprecipitation at a constant pH of 10 under vigorous stirring, and metallic salts solutions were prepared with M^{II}:Al^{III} molar ratios of 2 and 3 (only for Zn^{II}-Al^{III} LDH). M^{II}:Al^{III} molar ratios of materials, measured by ICP-MS, were found to be very close to the expected values **(Table S1)**. This implies that almost all the Al^{III} ions are co-precipitated with the M^{II} ions to obtain a solid with the stoichiometry of two or three M^{II} atoms for each Al^{III} atom, thus corresponding potentially to ideal arrangements of the M^{II} and Al^{III} cations in the brucite-like sheets **(Lieth, 1977)**.

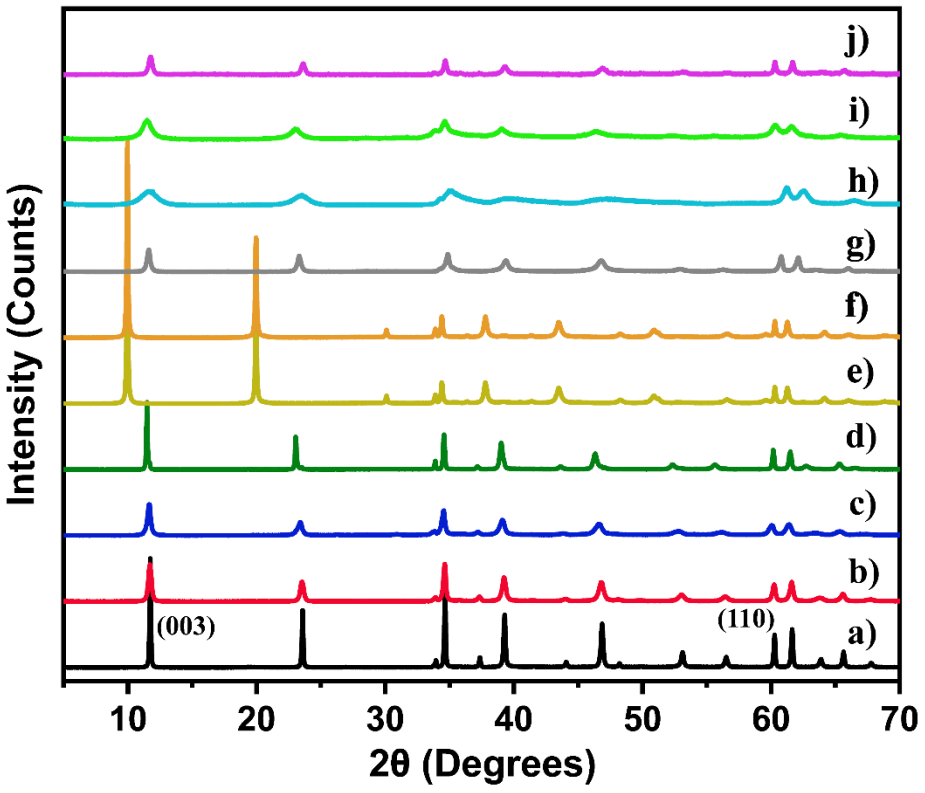

Figure 1. PXRD patterns of the different prepared LDH samples: a) Zn_2Al:CO_3-hyd, b) Zn_2Al:CO_3-cop, c) Zn_3Al:CO3, d) Zn_2Al:Cl, e)Zn_2Al:NO_3, f) Zn_2Al:ClO_4, g) Mg_2Al:CO_3, h) Cu_2Al:CO_3, i) Ni_2Al:CO_3, j) Co_2Al:CO_3.

Figure 1 shows the PXRD patterns of the prepared LDH samples having the characteristic reflections of layered double hydroxides exhibiting a hexagonal lattice with rhombohedral 3R symmetry **(Cavani et al., 1991)**. The low angle peak situated in the 2θ range 10° and 12° depending on the type of LDH is indexed to the (003) basal reflection, whereas the peak located at 2θ of approximately 60° is indexed to the (110) reflection. The unit cell lattice parameters *a* and *c* can be calculated from the position of these two peaks, with $a = 2d_{(110)}$ and $c = 3d_{(003)}$ **(Mahjoubi et al., 2017)**.

The obtained parameters as well as the crystallite sizes $L_{(003)}$ and $L_{(110)}$, calculated as XRD coherent domains in directions perpendicular to the (003) and (110) planes respectively using Scherrer's formula, are presented in **Table 1**. Slightly different lattice parameters of carbonate-intercalated LDH samples may be due to the different atomic radii of their constituent metals and their orientation within the LDH structure **(M. Li et al., 2020)**. The values of the crystallite sizes $L_{(003)}$ and $L_{(110)}$ show that the prepared LDHs exhibit a relatively good crystallinity, with an only exception for $Cu_2Al{:}CO_3$ sample. This was also shown in the PXRD pattern of $Cu_2Al{:}CO_3$ (**Figure 1-h**) which exhibited broader less intense diffraction peaks at (003) and (110) reflections caused by poor long-range ordering **(J. Li et al., 2017)**. Such decrease in crystallinity could be actually attributed to the Jahn-Teller distortion effect of copper present in octahedral coordination **(Kannan et al., 2004)**.

Table 1. Unit cell parameters, interlamellar distance (d), $L_{(003)}$ and $L_{(110)}$ of the prepared LDH samples. The data was calculated by using the peak positions and the full width at half maximum (FWHM) of the (003) et (110) diffraction peaks presented in Figure 1.

Sample	a (Å)	c (Å)	d (Å)	$L_{(003)}$* (nm)	$L_{(110)}$* (nm)
$Zn_2Al{:}CO_3$-hyd	3.06	22.59	7.53	69	60
$Zn_2Al{:}CO_3$-cop	3.07	22.65	7.55	27	32

Zn_2Al:Cl	3.07	23.1	7.7	46	32
Zn_2Al:NO_3	3.07	26.61	8.87	45	31
Zn_2Al:ClO_4	3.08	27.45	9.15	47	37
Zn_3Al:CO_3	3.08	22.86	7.62	25	35
Cu_2Al:CO_3	3.03	22.77	7.59	6	15
Ni_2Al:CO_3	3.05	22.59	7.59	13	23
Co_2Al:CO_3	3.05	22.56	7.52	23	37
Mg_2Al:CO_3	3.06	22.77	7.59	25	29

[*] Crystallite sizes calculated as XRD coherent domains in directions perpendicular to (003) or (110) planes using Scherrer's formula. The cell parameters were calculated by using the peak positions of the (003) et (110) diffraction peaks presented in Figure 1.

The *c* parameter of Zn^{II}-Al^{III} carbonate-intercalated LDHs were found to be very close to that found in the literature **(Crespo, 1997; J. Zhang et al., 2004)**. A slight difference could be noted between Zn_2Al:CO_3-hyd and Zn_2Al:CO_3-cop. A similar change in *c* lattice parameter was reported by Kovanda *et al.***(Kovanda et al., 2009)** and Benito *et al.***(Benito et al., 2006)** who assigned the decrease in the interlamellar space of the LDH after exposing it to hydrothermal treatment to the strengthening of the interaction between the interlayer anions and the hydroxide layers. As suggested by **Figure 1**, the application of hydrothermal treatment had also resulted in an increase of the integral intensity of (003) and (110) diffraction lines. This was associated with larger $L_{(003)}$ and $L_{(110)}$ crystallite sizes **(Table 1)**, which also indicates an enhancement in the crystallinity of LDH phase in the treated sample and further ordering of the LDH crystal structure **(Kovanda et al., 2009)**. Such effect of hydrothermal treatment on the crystallinity of the LDH samples is expected, where the application of hydrothermal treatment on hydrotalcites is mainly aimed to : (i) transform the small crystallites of the powders into larger more crystallized ones, (ii) transform amorphous precipitates into crystalline LDHs **(Cavani et al.,**

1991), or (iii) induce crystal rearrangement, thus decreasing the number of defects present in the crystals **(C.-C. Wang & Ying, 1999).** Miyata *et al.* had also reported a dramatic effect on the crystallite size induced by hydrothermal treatment of hydrotalcite compounds **(Miyata, 1980)**. Actually, thermal treatment promotes the continuous dissolving of a significant part of the less thermodynamically stable particles obtained during the coprecipitation step, *i.e.* small particles with high surface energy and amorphous phases, while the resulting dissolved species recrystallize again adding to and forming more stable crystals **(Galvão et al., 2016).**

On the other hand, upon increasing the molar ratio of Zn^{II}:Al^{III} from 2 to 3, an increase in the lattice parameters *a* and *c* was observed **(**

Table *2*). The first is related to the larger ionic radius of zinc compared to that of aluminum resulting in lattice expansion along the ab-plane, whereas the second is attributed to the reduction of layer electrostatic charge in the Zn_3Al:CO_3 LDH leading to wider interlayer distance along the c-axis **(Lee et al., 2016)**. Moreover, the crystallite sizes $L_{(003)}$ and $L_{(110)}$ had town down by 3 and 2 times, respectively. In fact, it had been previously reported that an increase in M^{II}:M^{III} molar ratio is usually associated with a reduction in crystallinity degree due to a decrease in layer charges **(Ahmed et al., 2013)**.

Moreover, upon exchanging carbonate anions in Zn_2Al:CO_3 with other anions, the type of XRD patterns was unchanged, indicating that the product still kept the rhombohedral 3R symmetry **(Y. Liu & Yang, 2016)**. However, the (003) peak was shifted to lower 2θ values compared with Zn_2Al:CO_3 LDH, revealing an increase in the crystal layer spacing *c*, following the order:

$$CO_3^{2-} < Cl^- < NO_3^- < ClO_4^-$$

The evolution of the *c* lattice parameter with the change in nature of intercalated anion is in agreement with those reported for hydrotalcite-like compounds **(Kloprogge et al., 2002; Bontchev et al., 2003),** thus indicating the success of the anion exchange reactions which was also ensured by Raman and IR spectroscopies. The interlamellar distance is actually related to the size, charge and orientation of the corresponding intercalated anions within the layers **(Mahjoubi et al., 2017)**. The effect of anion exchange of CO_3^{2-} with the other intercalating anions on the crystallinity of Zn_2Al LDHs had been also investigated. The results shown in **Table 1** provide an evidence about the sensitivity of the crystallinity of LDHs toward anion exchange reactions, where the crystallite sizes $L_{(003)}$ and $L_{(110)}$, had decreased by almost 1.5 times upon exchanging carbonate anions with chloride, nitrate and perchlorate. However, no

remarkable difference between the crystallite sizes of LDHs intercalated with Cl^-, NO_3^- and ClO_4^- was detected. We can thus assume that the exchange reactions of carbonate-intercalated LDHs, had led to a reduced crystallinity as a result of mechanical fragmentation of the crystallites rather than dissolution/recrystallization **(Salak et al., 2010)**. In fact, anion exchange reactions in layered double hydroxides involves the breakage of the electrostatic interactions as well as the hydrogen bonds between the hydroxide layers and the outgoing anion and the reformation of these bonds with the incoming anions **(Radha et al., 2005)**.

Finally, the purity of all the synthesized LDH powders was also checked out by Raman and IR spectroscopies, where no additional vibration bands assigned to amorphous phases have been detected **(Figures S1 and S2)**.

3.1.2. Textural features: Scanning Electron Microscopy imaging, BET specific surface area and Particle Size Distribution

As shown in **Figure 2**, $Zn_2Al{:}CO_3$-hyd and $Zn_2Al{:}CO_3$-cop as well as $Zn_3Al{:}CO_3$ LDH samples adopt a "cauliflower-like'' morphology, very similar to that reported by Scarpellini *et al.* **(Scarpellini et al., 2014)**. The scaled samples exhibited distinct platelet like particles in a high degree of agglomeration, which is a well-known characteristic of LDHs **(Clark et al., 2019)**.

In the absence of any hydrothermal treatment, the platelets hexagonal geometry of $Zn_2Al{:}CO_3$-hyd was less sharp and defined **(Figure 2c,d)** than that of $Zn_2Al{:}CO_3$-hyd. This highlights the lower crystallinity of the particles of $Zn_2Al{:}CO_3$ unexposed to any hydrothermal treatment. However, the lateral particle size of hydrothermally treated $Zn_2Al{:}CO_3$ (1050 ± 130 nm) was only slightly larger than that of the hydrothermally untreated sample (821 ± 112 nm). Thus, the larger crystallite size for $Zn_2Al{:}CO_3$-hyd did not lead to significant changes on the particle size at

383 the micrometric range. In fact, it has been previously reported that the lateral size of LDHs
384 prepared directly by coprecipitation without further hydrothermal treatment was almost the same
385 as that of LDHs subsequently exposed to hydrothermal treatment, although their coherent
386 crystallite domains were more than two times greater that of hydrothermally treated LDH
387 **(Hibino, 2014)**. On the other hand, Sun *et al.* reported a slight increase in the size of carbonate
388 intercalated LDH nanoparticles upon exposing it to a hydrothermal treatment at 85˚C for 7 hours
389 **(Sun & Dey, 2015)**. On the other hand, the SEM micrographs of $Zn_3Al{:}CO_3$ hexagonal platelets
390 having an average size lateral size 415 ± 45 nm, is much smaller and less defined than those of
391 $Zn_2Al{:}CO_3$. In this case, the reduction in the average lateral size is in good agreement with the
392 reduced coherent size of $Zn_3Al{:}CO_3$ **(Table 1).**

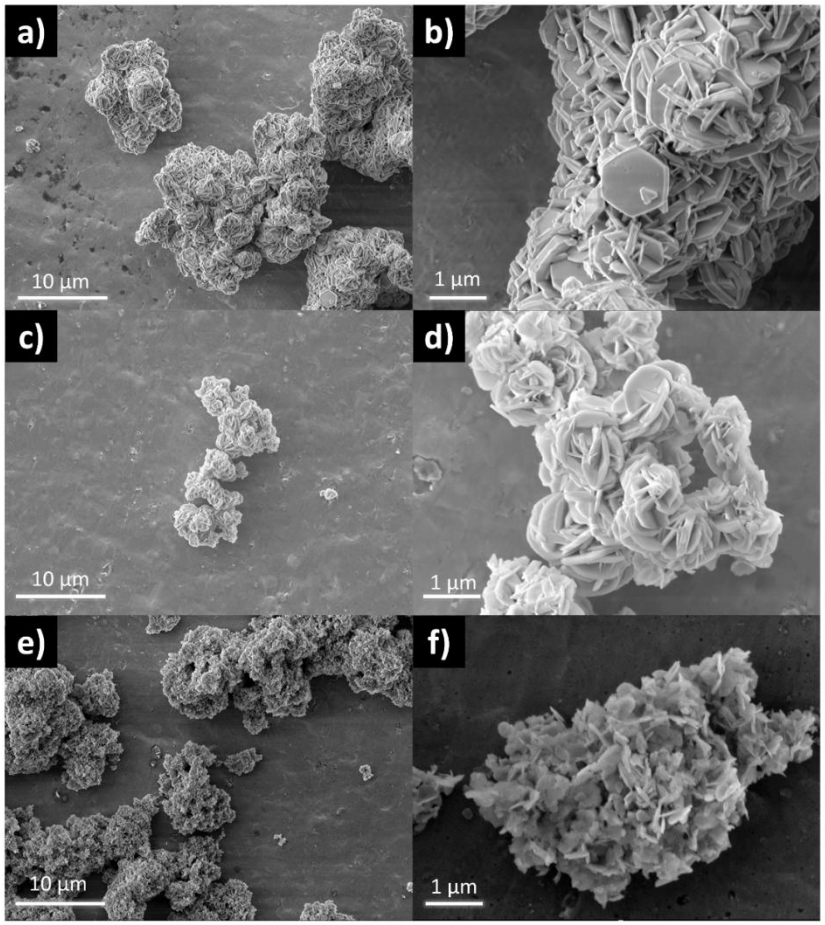

393

Figure 2. SEM micrographs of: a,b)$Zn_2Al:CO_3$-hyd, c,d) $Zn_2Al:CO_3$-cop, e,f) $Zn_3Al:CO_3$.

Moreover, upon exchanging carbonate anions in $Zn_2Al:CO_3$-hyd with chloride, nitrate and perchlorate anions a remarkable change in the morphology and aggregate size was observed **(Figure S3)**. The generation of defects in anion exchanged powders, especially for $Zn_2Al:NO_3$ and $Zn_2Al:ClO_4$, comes in line with the reduced crystallite sizes **(Table 1),** and suggests again the occurrence of mechanical fragmentation of the crystallites in an ion exchange reaction rather than dissolution/recrystallization **(Salak et al., 2010)**.

Figure 3 shows the morphology of $Cu_2Al:CO_3$ exhibiting small globular distorted crystallites with uncertain length, similar to that of CuMgAl LDH obtained by Oliveira *et al.* **(Rocha Oliveira et al., 2015)**. In general, the synthesis of LDH containing Cu^{II} as the only divalent metal is somehow difficult due to the Jahn teller distortion phenomena **(H. Liu et al., 2010)** which may had led to a distortion and presence of defects in its structure, as suggested by its PXRD pattern.

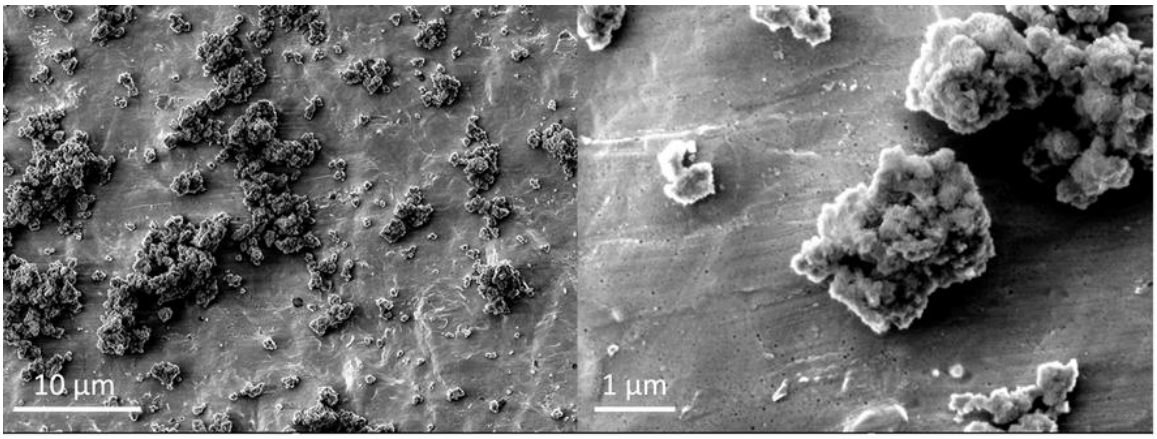

Figure 3. SEM micrographs of Cu2Al:CO_3 LDH.

The dissolution behavior of LDHs is considered as a surface-controlled reaction which is expected to be highly determined by their particle size **(Rojas, 2016)**. For this reason, the

specific surface area and particle size distribution of the synthesized different Zn^{II}-Al^{III} LDHs were studied by BET approach and Laser Diffraction, respectively.

BET provides a suitable method to measure specific surface area of LDH powders which is directly linked to their sizes. Moreover, particle size distribution (PSD) also gives information about the LDH particle sizes, which usually are aggregates of crystallites **(Herrero et al., 2008)**. The D_{v50} is the volume median diameter which divides the population exactly into two equal halves, whereas the $D_{[3,\ 2]}$ is the surface area mean diameter, which is more relevant when specific surface area is important, e.g. bioavailability, reactivity and dissolution **(Rawle, 2003)**. The specific surface areas of Zn^{II}-based LDHs determined by BET (S_{BET}), D_{v50} and $D_{[3,\ 2]}$ values are reported in

Table *2*.

Table 2. Specific surface area determined by BET , D_{v50} and $D_{[3,2]}$ determined by PSD for the different prepared Zn^{II}-Al^{III} LDH samples. The PSD curves are presented in Figure 4.

Sample	S_{BET} ($m^2.g^{-1}$)	D_{v50} (µm)	$D_{[3,2]}$ (µm)
$Zn_2Al:CO_3$-hyd	6.2	13.7±0.4	13.2±0.3
$Zn_2Al:CO_3$ -cop	19	9.6±0.3	5.2±0.2
$Zn_3Al:CO_3$	13.3	9.4±0.3	7.3±0.2
$Zn_2Al:Cl$	16.7	8.4±0.1	6.4±0.1
$Zn_2Al:NO_3$	22.5	3.1±0.1	2.6±0.1
$Zn_2Al:ClO_4$	24.8	1.7±0.1	1.5±0.1

Compared to $Zn_2Al:CO_3$-hyd LDH sample, which showed a monomodal narrow size distribution of particle aggregates having a median diameter of 13.7 µm **(Figure 4a)**, $Zn_2Al:CO_3$-cop showed a bimodal size distribution composed of both individual particles and aggregates with broader size distribution having an average median size of 9.6 µm **(Figure 4b)**. The larger size and narrow particle distribution of $Zn_2Al:CO_3$-hyd sample could be explained by the aging in hydrothermal conditions which leads to recrystallization and Ostwald ripening processes **(Rojas, 2016)**. Additionally, the larger S_{BET} and smaller $D_{[3,2]}$ for $Zn_2Al:CO_3$-cop supported such results. The reduction of the surface area of LDHs subsequently exposed to a hydrothermal treatment could be attributed to the recrystallization of small crystallites and amorphous particles and subsequent increase of the LDH crystallite size **(Kovanda et al., 2009)**, which is also confirmed by our XRD and SEM results presented in **Figure 1** and **Figure 2**, respectively.

On the other hand, upon increasing the molar ratio of Zn^{II}:Al^{III} from 2 to 3, the LDH powder showed a broader particle size distribution. $Zn_3Al:CO_3$ exhibited a monomodal distribution similar to that of $Zn_2Al:CO_3$, yet with a short arm located at around 100 µm and a smaller aggregated particles fraction (~27%) in the range of 1.5-5 µm (**Figure 4c)**, which was absent in the case of $Zn_2Al:CO_3$-hyd.

Similarly, upon exchanging carbonate anions in $Zn_2Al{:}CO_3$ with other intercalating anions, *i.e.* Cl^-, NO_3^-, and ClO_4^-, a significant fraction of smaller agglomerates and/or individual particles appeared (**Figure 4d,e,f)**. Such decrease in agglomeration degree imposed by anionic exchange reactions could also be seen through the SEM micrographs presented in **Figure S3**. This was also associated with a remarkable increase in S_{BET} and smaller D_{V50} and $D_{[3,2]}$ sizes, especially for the nitrate and perchlorate intercalated samples (

447 **Table *2***).

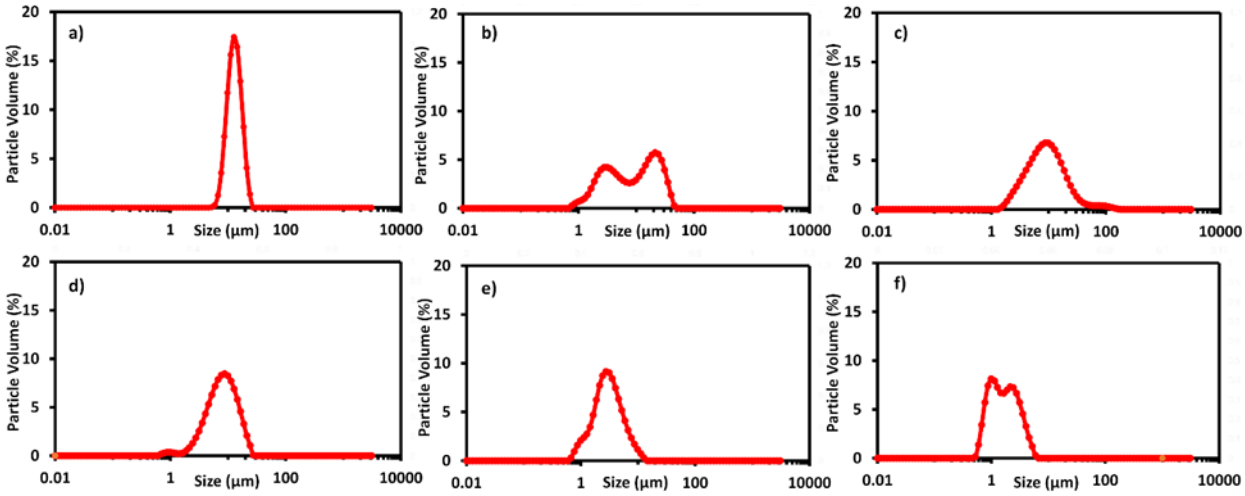

448

449 **Figure 4.** Particle Size Distribution (PSD) curves in water dispersion of: a) $Zn_2Al:CO_3$-hyd, b) $Zn_2Al:CO_3$-cop, c)
450 $Zn_3Al:CO_3$, d) $Zn_2Al:Cl$, e) $Zn_2Al:NO_3$, and f) $Zn_2Al:ClO_4$.

451 ### 3.2.Metal partial dissolution experiments

452 The partial dissolution of all the synthesized LDH powders into Al^{III} and their constituent
453 divalent metals M^{II} in LB and TSB liquid broth media, of pHs 6.7 and 7 respectively, was
454 studied after 48 h of incubation at 37°C. The negative blanc tests of pure LB and TSB media
455 ensured that the media where the study had taken place did not contain any amounts of Al^{III} or
456 any other divalent metal included in the study, *e.g.*, Zn^{II}, Cu^{II}, Ni^{II}, Co^{II}, Mg^{II}, prior to the
457 addition of LDH powders. The partial dissolution profiles of all synthesized LDH samples are
458 revealed in **Figure 5**.

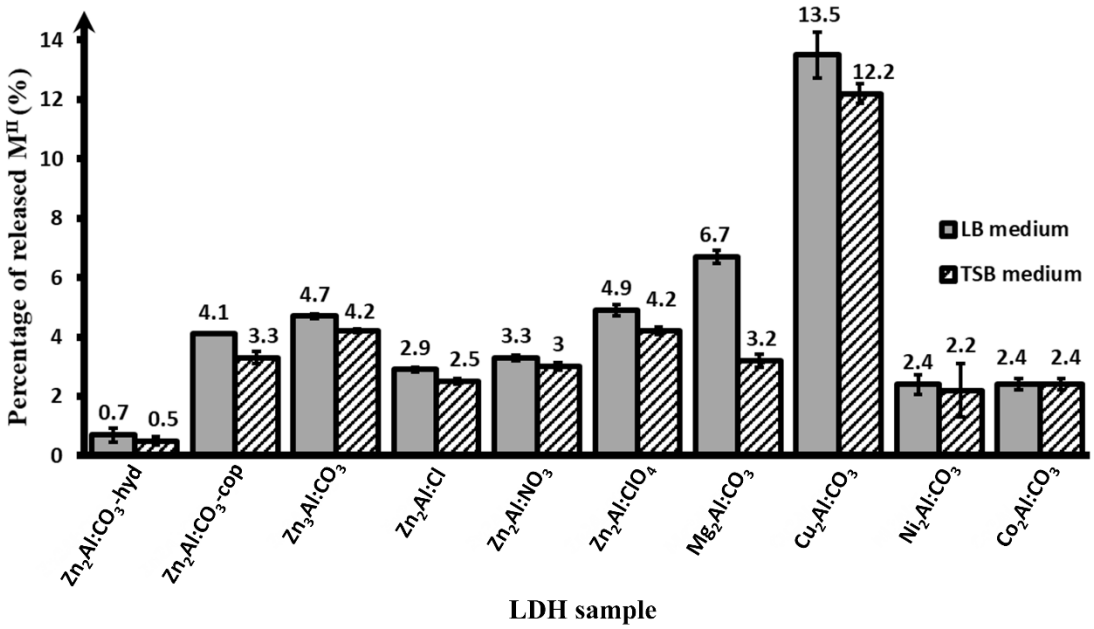

Figure 5. Partial dissolution profiles of all synthesized LDH samples into M^{II} in LB and TSB media in terms of average percentage compared to the initial amount present in the LDH.

In this study, the dissolution of LDHs into their constituent divalent metals was uniquely considered, since the dissolution of Al^{III} in both LB and TSB media were below the detection point for all the tested samples. In fact, Peng *et al.* had previously shown that only divalent cations were released from LDH powders into a certain biological medium (α-MEM), whereas soluble trivalent cations (Al^{III} and Fe^{III}) were not released **(Peng et al., 2018)**. Jobbagy *et al.* also reported that the dissolution of Al^{III} out of Mg_2Al:Cl LDH was below the limit of detection in the range $5 \leq pH \leq 9.0$, and only leaching of Mg^{II} was observed **(Jobbágy & Regazzoni, 2011)**.

Control partial dissolution experiments of the synthesized LDH powders were also done in Milli-Q distilled water having a pH of 6.98 very close to that of LB and TSB, where the release of both divalent and trivalent metals was below the detection point for all the LDH samples **(Table S2)**. Such behavior could provide an evidence that the chemical species contained in LB and TSB broth are able to increase the solubility of LDHs by the formation of complex species with their

constituent divalent metal. In fact, several studies have previously shown that the solubility and metal release from zinc oxide (ZnO) powders was greatly enhanced in biological complex media as LB, TSB and MH (Mueller Hinton) broths, which may be due to the ability of zinc present in the powder to react with amino acids and proteins to form complex organometallic compounds **(Esteban-Tejeda et al., 2017; S. Liu et al., 2014; Pasquet et al., 2014)**. In the present case, proteins and amino acids present in LB and TSB liquid broths were probably the chemical species that might formed complexes with M^{II} ions and provided a superior dissolution of the powders compared to that in water.

Furthermore, in order to ensure that thermodynamic equilibrium was reached within 48 hours of LDH dispersion incubation, the evolution of Zn^{II} released from Zn_2Al:CO_3-hyd and Zn_2Al:CO_3-cop was monitored over time. As suggested by **Figure S4**, thermodynamic equilibrium was reached for Zn_2Al:CO_3-hyd and Zn_2Al:CO_3-cop within 8 and 6 hours, respectively. The faster release profile in Zn_2Al:CO_3-cop was probably due to the presence of a significant fraction of smaller particles/agglomerates **(Figure 4)** which had provided a larger exposed surface area in contact with the dissolution media, thus promoting greater release of Zn^{II} in aqueous broth solutions **(Rojas, 2016)**.

Thus, the following subsections mainly focus on the effect of different parameters, *e.g.* crystallinity, M^{II}:Al^{III} molar ratio, type of intercalated anion and nature of divalent metal and M^{II}:Al^{III} on the partial dissolution of different LDHs into their corresponding constituent divalent metals in LB and TSB aqueous dispersions.

3.2.1. Effect of crystallinity in Zn_2Al:CO_3

The application of a post-synthetic hydrothermal treatment is an important step evaluated in this study for obtaining Zn_2AlCO_3 LDH samples having different crystallinities: Zn_2Al:CO_3-hyd and Zn_2Al:CO_3-cop. Both samples were prepared using the same experimental procedures, where the only difference was the application of a hydrothermal treatment for Zn_2Al:CO_3-hyd, while Zn_2Al:CO_3-cop was not exposed to any post-synthetic treatment procedure. Subsequently, the two LDHs possessed different structural and textural properties, where Zn_2Al:CO_3-cop exhibited lower crystallinity revealed by their smaller crystallite sizes **(Table 1),** larger surface area, smaller median size and surface area mean of agglomerates **(**

503 **Table *2*)** than those of the treated one.

504 The crystallinity effect on the stability and dissolution properties of LDHs was studied by
505 evaluating the amount of released Zn^{II} from hydrothermally treated and untreated $Zn_2Al{:}CO_3$
506 LDH samples in LB and TSB media. It could be noticed from **Figure 5**, that the dissolution of
507 Zn^{II} in both samples was slightly higher in LB medium than TSB. This might be simply
508 attributed to the difference in nature and composition of the biological growth media, in addition
509 to the slightly lower pH of LB (6.63) compared to that of TSB (6.97), where it is known that the
510 solubility of LDHs is highly pH-dependent and their dissolution accelerates with increasing
511 acidity **(Zheng et al., 2013)**.

512 In both media, the amount of the leached Zn^{II} out of $Zn_2Al{:}CO_3$-cop was enhanced by almost 6
513 times in comparison to that of $Zn_2Al{:}CO_3$-hyd. Such result is consistent with that of Hibino, who
514 found out that the release of Mg^{II} out of lower crystallinity Mg^{II}-Al^{III} LDH directly obtained after
515 co-precipitation was higher than that of the same LDH subsequently exposed to hydrothermal
516 treatment **(Hibino, 2014)**. Therefore, the lower crystallinity of Zn^{II}-Al^{III} LDH as well as their
517 smaller aggregated sizes and larger surface area promotes the release of more Zn^{II} ions in broth
518 culture media.

519 ### 3.2.2. Effect of $M^{II}{:}Al^{III}$ molar ratio in $Zn_2Al{:}CO_3$ LDHs

520 The impact of $M^{II}{:}M^{III}$ molar ratio on divalent metal dissolution capacity of LDHs was another
521 important parameter investigated in our study, by which as far as our knowledge such impact
522 have not been studied before. Such influence was examined by comparing the partial dissolution
523 profiles of Zn^{II} of the two prepared LDH samples: $Zn_2Al{:}CO_3$-hyd and $Zn_3Al{:}CO_3$ having a

524 $Zn^{II:}Al^{III}$ molar ratio of 2 and 3 respectively. The two samples were prepared using a similar
525 coprecipitation experimental procedure followed by a hydrothermal treatment at 80°C.

526 As shown in **Figure 5**, the partial dissolution profiles of Zn^{II} increases significantly by about 7
527 and 8 times in LB and TSB media respectively, when the molar ratio of Zn^{II}:Al^{III} was increased
528 from 2 to 3.

529 It is worth mentioning here that the crystallinity of these samples and the particles/agglomerates
530 sizes as well their surface areas were not the same for these two samples. The crystallite sizes
531 determined by XRD **(Table 1**Erreur ! Source du renvoi introuvable.**)** were reduced by at least
532 two times upon increasing the Zn^{II}:Al^{III} molar ratio. It was actually noticed in the previous section
533 that the crystallinity of LDHs could play an important role on their dissolution behavior, where
534 the solubility of LDHs in aqueous solutions was expected to be enhanced as their crystallinity
535 decreases **(Section 3.2.1)**. Thus, the higher dissolution behavior presented in Zn_3Al:CO_3 could be
536 either assigned to its higher zinc content initially present in the structure, or to its lower
537 crystallinity, or to the combined effect of these two factors.

538 **3.2.3. Effect of intercalated anion**

539 The influence of intercalating four different interlayer anions: CO_3^{2-}, Cl^-, NO_3^- and ClO_4^- in
540 Zn_2Al LDH layers, on their partial dissolution into Zn^{II} ions was investigated. The partial
541 dissolution profiles of these LDHs **(Figure 5)**, prove that changes in the nature and composition
542 of the anion in the hydrotalcite interlayer region exhibited an important effect on the solubility of
543 $Zn^{II-}Al^{III}$ LDHs. For instance, the release of Zn^{II} increases by about 4 times in LB medium upon
544 exchanging carbonate anions with chloride and nitrate ones, and 6 times in case of perchlorate
545 compared to carbonate intercalated sample within the same LB medium. Another important point

to note here is that the difference in the dissolution behavior in LB and TSB media, having slightly different pHs, is more pronounced in case of carbonate intercalated Zn_2Al LDH than other samples having other intercalated anions. This could be explained by the urge to protonate both hydroxyl groups and carbonate anions in order for the dissolution to occur in carbonate intercalated LDH **(Hibino, 2014)**, thus making Zn_2Al:CO_3 LDH sample more sensitive to the pH of the aqueous media.

It is also remarkable that the increasing solubility of LDHs here followed the same trend as that of the value of c parameter obtained by XRD **(Section** Erreur ! Source du renvoi introuvable.**)**, and the opposite trend to that of the order of affinity of LDHs toward intercalating anions previously described in the literature **[27,28]**:

$$CO_3^{2-} > Cl^- > NO_3^- > ClO_4^-$$

Thus, one could conclude that the lower the affinity of the intercalated anion toward the Zn_2Al LDH structure, the lower the stability of the LDH in broth media.

In fact, some previous studies showed that the dissolution of LDHs was strongly dependent on the type of intercalated anion, where Baek *el al.* reported that chloride intercalated MgAl-LDH was less stable and released more magnesium ions than carbonate intercalated MgAl-LDH in simulated body conditions **(Baek et al., 2011)**. Other theoretical thermodynamic study had also shown that NO_3^- intercalated hydrotalcites were more soluble than CO_3^{2-} intercalated ones and even small amounts of carbonate could change the solubility of a nitrate phase by several orders of magnitude **(R. k. Allada, 2002)**.

However, one important parameter neglected by these studies **(Allada, 2002; Baek et al., 2011)**, is the difference in crystallinity and the structure of the LDHs having different intercalated

anions. As previously mentioned in **Section 3.1.1**, exchanging carbonate anions in Zn_2Al LDHs with other anions less favored by the LDH structure promoted a remarkable decrease in the crystallinity of the latter associated with a decrease in aggregate sizes **(**

Table *2*) and generation of defects in the structure **(Figure S3)**.

Therefore, the poor crystallinity and presence of defects in Zn_2Al LDHs is a first explanation for the higher dissolution of LDHs obtained by anion exchange. The second one is the nature of intercalated anion itself, which may weaken the binding between the metal cations and the layers, thus promoting higher dissolution behavior.

3.2.4. Effect of divalent metal

In order to examine the relationship between the constituent divalent metal M^{II} of the LDHs and their dissolution properties, different LDHs having a molar ratio of M^{II}:Al^{III} =2 were synthesized coprecipitation method followed by a hydrothermal treatment at 80°C for 24 hours. The intercalated anion in all these LDH samples was CO_3^{2-}, and the divalent metal was changed accordingly: M^{II}= Zn^{II}, Mg^{II} Cu^{II}, Ni^{II}, or Co^{II}.

According to **Figure 5**, the partial dissolution profile of $M_2Al:CO_3$ LDHs into M^{II} in both LB and TSB media followed the following trend:

$$Cu_2Al:CO_3 > Mg_2Al:CO_3 > Co_2Al:CO_3 \simeq Ni_2Al:CO_3 > Zn_2Al:CO_3$$

Table S3 provides the relative p*K*sp values of the different divalent metal hydroxides counterparts of the different synthesized LDH samples. In fact, Boclair *et al.* had previously related the relative stabilities of LDHs to their corresponding metal hydroxides **(Boclair & Braterman, 1999)**. That is for a given M^{II} cation, the higher the solubility of $M^{II}(OH)_2$, the less stable its corresponding LDH is. Thus, we tried to correlate the solubility of $M^{II}(OH)_2$ to the partial dissolution profiles of divalent metals from $M_2Al:CO_3$ in LB and TSB media. Our results agreed well with the proposed hypothesis by Boclair *et al.*, by which lower dissolution is

observed with increasing $M^{II}(OH)_2$ p*K*sp values. The dissolution driving force is dictated by thermodynamics, and the solubility of LDHs varies according to the nature of the constituent metal ions. One sole exception was noted in the case of $Cu_2Al{:}CO_3$ LDH which seemed to be highly unstable thus generating an amplified release of Cu^{II} although $Cu(OH)_2$ exhibited lower solubility compared to those of the other studied divalent metals. This surprising result, may be attributed to the poor crystallinity of $Cu_2Al{:}CO_3$ **(Figure 1.h)**, very small crystallite sizes ($L_{(003)}\approx$ 6nm and $L_{(110)}\approx$ 15 nm), and its distorted very irregular structure revealed by its SEM micrographs (**Figure 3**), thus indicating the presence of defects due to Jahn Teller distortion phenomena.

3.3.Antibacterial activity

3.3.1. Influence of nature of divalent metal on antibacterial activity

The antibacterial activities of the different prepared LDH samples were conducted against both Gram-positive and Gram-negative bacterial strains, *S. aureus* and *E. coli* respectively, using the agar disk diffusion method. The antimicrobial activity tests were also done using metallic salts solutions as references. The generated inhibition zones of some LDH samples against both tested bacteria are displayed in **Figure 6**.

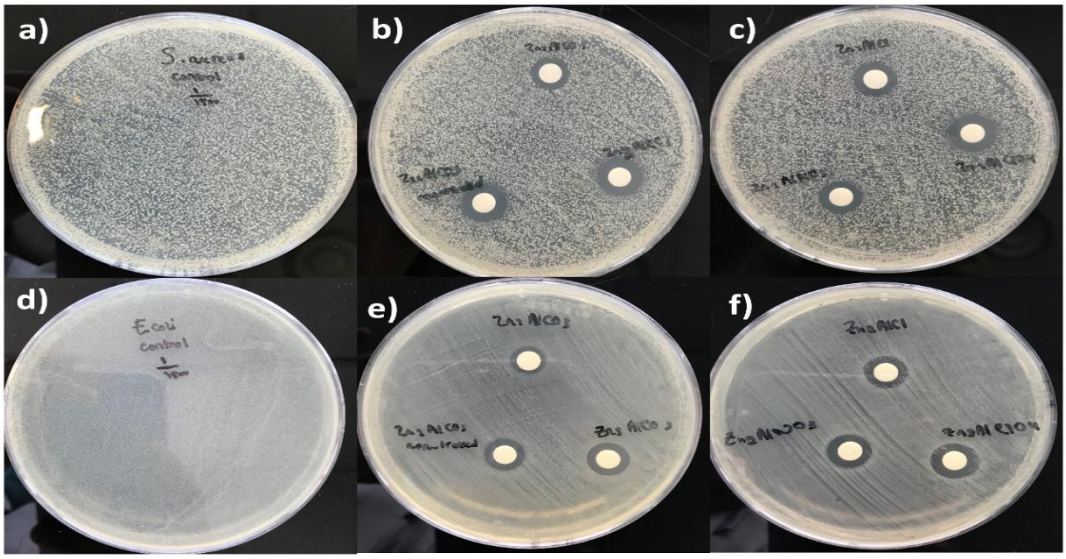

Figure 6. Antibacterial agar disk diffusion tests against: a) *S. aureus* control, b) *S. aureus* using $Zn_2Al:CO_3$-hyd (top), $Zn_2Al:CO_3$-cop (bottom left) and $Zn_3Al:CO_3$ (bottom right), c) *S. aureus* using $Zn_2Al:Cl$ (top), $Zn_2Al:NO_3$ (bottom left) and $Zn_2Al:ClO_4$ (bottom right), d) *E. coli* control, e) *E. coli* using $Zn_2Al:CO_3$-hyd (top), $Zn_2Al:CO_3$-cop (bottom left) and $Zn_3Al:CO_3$ (bottom right), f) *E. coli* using $Zn_2Al:Cl$ (top), $Zn_2Al:NO_3$ (bottom left) and $Zn_2Al:ClO_4$ (bottom right).

As shown in **Figure 7**, only Zn^{II} and Cu^{II}-based LDHs were able to impose an antimicrobial effect against *E. coli* and *S. aureus*. Zn^{II}-based LDHs provided inhibition zone diameters ranging from 7 to 13 mm depending on the type of LDH and the amount of zinc ions released. These obtained values were similar to those found for pristine LDHs prepared Li et al. **(M. Li et al., 2020)** and Mishra *et al.* **(Mishra et al., 2018).** However, other antimicrobial pristine Zn^{II}-based LDHs possessed greater bacterial inhibition zones **(Dutta et al., 2020; Moaty et al., 2016)**. Such difference in the antimicrobial performance may be related to the properties of the tested LDHs, the different tested bacterial strains, the applied LDH dosage as well as to the different way the antimicrobial agar diffusion test assay was carried out.

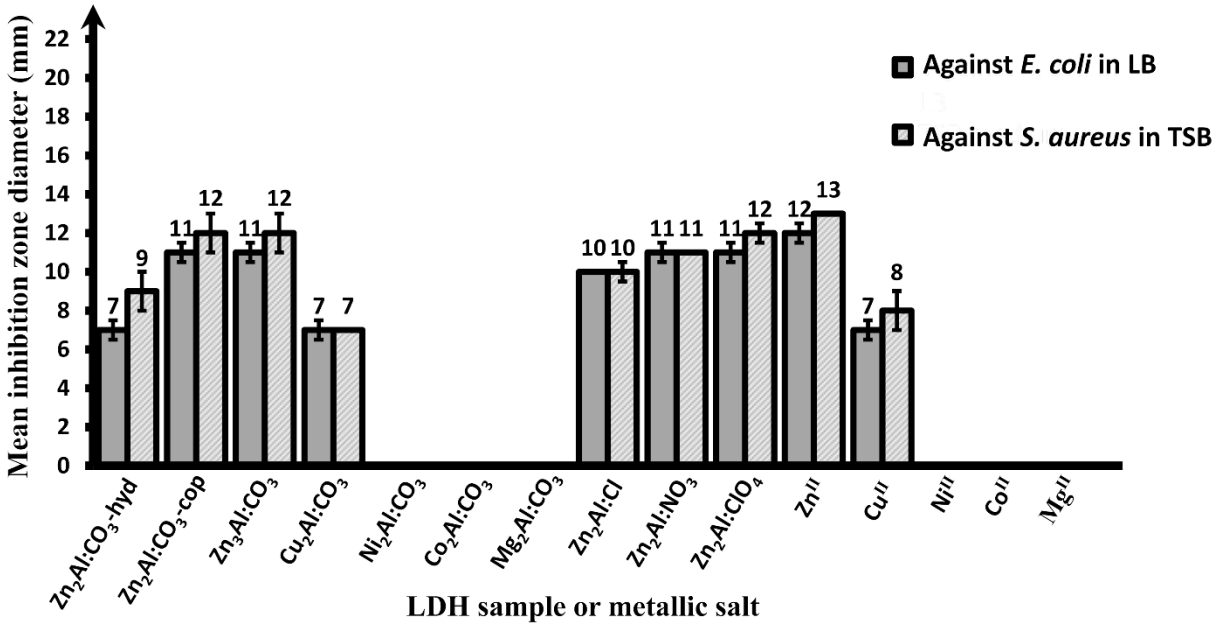

Figure 7. Antimicrobial activity of LDH samples and metallic ion solutions against *S. aureus* and *E. coli* in terms of mean zone of inhibition.

In fact, previous studies had established the capability of pristine Zn^{II}-containing LDH powders to act as efficient antimicrobial materials **(Moaty et al., 2016; Peng et al., 2018)**. Another recent study had also demonstrated that modified as well as unmodified Cu^{II}-based hydrotalcites could exhibit a bactericidal effect that is expected to be dependent on the amount of released copper ions **(Rocha Oliveira et al., 2015).**

Therefore, the antibacterial activity of pristine LDHs is primarily dependent on the nature of constituent divalent metals where Zn^{II}-based LDHs performed best in the agar disk diffusion test assay followed by Cu^{II}-based LDH sample.

3.3.2. Difference in antibacterial activity between Zn^{II} and Cu^{II}-based LDHs

The fact that Zn^{II}-containing LDHs were able to establish a superior antibacterial activity to those of other LDHs, even at low Zn^{II} release profile as is the case for Zn_2AlCO_3-hyd, could be attributed to the nature of the divalent metal present in the LDH itself. Where the tested Zn^{II} salts

638 also showed an enhanced antibacterial activity in comparison with the Cu^{II} salts **(Figure 7)**. This
639 highlights again the specificity of the antimicrobial effect toward the nature of the divalent metal.
640 Indeed, both Zn^{II} and Cu^{II} metallic ions possess similar antibacterial mechanisms by which they
641 can cause damages to membrane functions by blocking the transport of nutrients and substances
642 in and out the membrane, or bind to bacterial intracellular DNA leading to their denaturation
643 **(Borkow & Gabbay, 2005; Mittapally et al., 2018; Peng et al., 2018)**. However, the difference
644 in the antimicrobial efficiency between different divalent metals, in this case Zn^{II} and Cu^{II}, is
645 actually dependent on several factors, including the role each metal plays in normal metabolism,
646 and the presence of specific binding sites for each metal **(Borkow & Gabbay, 2005)**. Therefore,
647 microorganisms may be more sensitive to one metal than the other **(Bruins et al., 2000)**, *i.e.* in
648 this case *E. coli* and *S. aureus* were more sensitive to Zn^{II} than Cu^{II}.

649 ### 3.3.3. Influence of the solubility of LDHs on its antibacterial activity

650 Based on the proposed antibacterial mechanisms of LDHs provided in **Table 3**, the antimicrobial
651 activity of LDHs may be due to: (i) electrostatic surface interactions with the negatively charged
652 bacterial membranes, (ii) generation of biological toxic reactive oxygen reactive species (ROS),
653 (iii) release of antimicrobial metallic ions. Taking the third mechanism specifically into
654 consideration, the inability of Ni^{II} and Co^{II}-based LDHs to demonstrate an antibacterial activity
655 could be explained by the lower release profiles of Ni^{II} and Co^{II} out of Ni_2AlCO_3 and Co_2AlCO_3
656 LDHs respectively. Their respective metallic salts were also not able to impose the desired
657 antimicrobial effect at a concentration similar to that of the released ones. Whereas in case of
658 Cu_2AlCO_3, the release profile of Cu^{II} was remarkably high (in the range of 10 $mmol.L^{-1}$) thus

providing a sufficient concentration to inhibit the growth of *E. coli* and *S. aureus* in LB and TSB, respectively.

Table 3. Antimicrobial performance of pristine LDHs and the proposed antibacterial mechanisms by the literature.

Pristine LDH	Tested bacteria	Inhibition zone diameter (mm)	MIC ($mg.mL^{-}$)	Antimicrobial Performance	Proposed mechanism	Reference
$Zn_2Al:CO_3$ $Zn_2Al:Cl$ $Zn_2Al:NO_3$ $Zn_2Al:ClO_4$ $Zn_3Al:CO_3$ $Cu_2Al:CO_3$ $Co_2Al:CO_3$ $Cu_2Al:CO_3$ $Ni_2Al:CO_3$ $Mg_2Al:CO_3$	Gram-positive: *Staphylococcus aureus* Gram-negative: *Escherichia coli*	7-13	0.375-12	Depending on the nature of divalent metal (highest activity for Zn^{II}-based LDHs) and amount of released Zn^{II} in broth media initially dependent on different paramters (crystallinity, Zn^{II}:Al^{II}molar ratio, nature of intercalating anion)	Metal ion release	**This study**
$Zn_2Al:CO_3$	Gram-positive: *Staphylococcus aureus, Streptococcus lactis, Bacillus cereus* Gram-negative: *Pseudomonas aeruginosa, Escherichia coli, Salmonella typhimurium*	9-21	0.15-0.3	Depending on the applied LDH dosage and type of tested bacteria	Surface interactions, generation of ROS, metal ions release	**(Dutta et al., 2020)**
$Cu_2Al:CO_3$ $Ni_2Al:CO_3$ $Co_2Al:CO_3$ $Mn_2Al:CO_3$ $Mg_2Al:CO_3$	Gram-positive: *Staphylococcus aureus* Gram-negative: *Escherichia coli*	>10	0.8-1.5	Depending on the type of divalent metal: highest activity for $Mn_2Al:CO_3$ and $Cu_2Al:CO_3$, minimal activity for $Ni_2Al:CO_3$ and $Co_2Al:CO_3$, no activity for $Mg_2Al:CO_3$	Surface interactions, generation of ROS, metal ions release	**(M. Li et al., 2020)**
Ternary $CuMgAl:CO_3$	Gram-positive: *Staphylococcus aureus, Enterococcus faecalis, Bacillus Subtilis* Gram-negative: *Escherichia coli, Pseudomonas aeruginosa*	–	0-31	Increasing antibacterial activity with increasing Cu^{II}:Al^{II} molar ratio	Surface interactions, generation of ROS	**(Tabti et al., 2020)**

$Zn_2Al:CO_3$ $Zn_3Al:CO_3$ $Zn_4Al:CO_3$	Gram-positive: *Staphylococcus epidermidis*, *Staphylococcus aureus* *Gram-negative : Pseudomonas aeruginosa*	–	4-10	Increasing antibacterial activity with increasing Zn^{II}:Al^{II} molar ratio	Metal ions release, generation of Reactive Oxygen Species (ROS)	**(Lobo-Sánchez et al., 2018)**
Ternary $CuZnAl:SO_4$	Gram-positive: *Staphylococcus aureus* Gram-negative: *Escherichia coli*	8-15	100-310	Depending on the applied LDH dosage	Surface interactions, metal ions release	**(Mishra et al., 2018)**
$Zn_2Fe:NO_3$	Gram-positive: *Staphylococcus epidermidis*, *Staphylococcus aureus*, *Streptococcus pyogenes* Gram-negative: *Proteous vulgaris*, *Klebsiella pneumoniae*, *Escherichia coli*, *Pseudomonas aeruginosa*	16.8-22.9	–	Depending on the type of tested bacteria and selectivity of LDHs toward different bacterial strains	(Moaty et al., 2016)	**(Moaty et al., 2016)**

Furthermore, the relationship between the solubility of Zn^{II}-based LDH in bacterial growth media and their antimicrobial properties was established. For this purpose, the evolution of the minimum inhibitory concentration (MIC) of Zn^{II}-based LDH samples determined in liquid LB and TSB broths, was studied as a function of the percentage of released amount of Zn^{II} out of them, *i.e.* $Zn_2Al:CO_3$-hyd, $Zn_2Al:CO_3$-cop, $Zn_3Al:CO_3$ $Zn_2Al:Cl$, $Zn_2Al:NO_3$, $Zn_2Al:ClO_4$, prepared using different experimental procedures. According to **Figure 8**, the obtained MIC values ranged from 0.375 to 12 $mg.mL^{-1}$ depending on the type of Zn^{II}-based LDH used and the amount of zinc ions it released. The obtained MIC values fall within the range of the obtained MIC values for most pristine antimicrobial LDHs found in the literature with some slight differences depending on the way the MIC was evaluated and the properties of tested LDHs **(M. Li et al., 2020; Lobo-Sánchez et al., 2018; Z. Wang et al., 2018)**. The MIC values of Zn^{II}-based LDH samples decreased significantly depending on the amount of released Zn^{II} in broth

media **(Figure 8)**. This points out the impact of the dissolution phenomenon of Zn^{II}-Al^{III} LDH powders on their antibacterial efficiency, by which the antimicrobial activity is enhanced with increasing solubility and divalent metal release profiles of their constituent divalent metal. This finding supports the possible mechanism of the antibacterial activity of LDHs induced by the release of their constituent metallic ions. In other words, when present in aqueous solutions, Zn^{II}-containing LDHs release Zn^{II} into the medium, where it can act as an inorganic antibacterial agent, thus inhibiting the growth of the bacteria. Zn^{II} soluble species then may damage the bacterial membrane function through changing its charge distribution thus blocking the transport of substances in and out of the membrane or else by binding to nucleic acids leading to bacterial proliferation inhibition **(Peng et al., 2018)**.

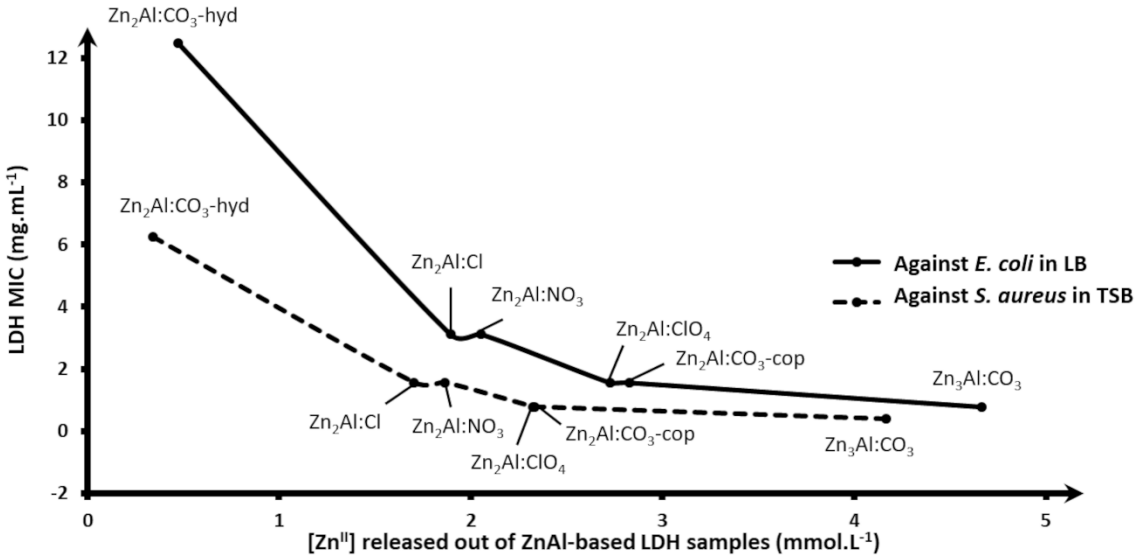

Figure 8. Evolution of antimicrobial activity in terms of LDH MIC against *S. aureus* and *E. coli* as a function of average dissolution of Zn^{II} out of Zn-based LDH samples.

It is also remarkable here to mention that the antibacterial efficiencies of both LDH powders dispersions and metallic ion salts were more pronounced against S. aureus than *E. coli*, although the release profile of divalent metals was higher in LB medium than in TSB. This could be

simply linked to the specificity of the antimicrobial agents toward a certain bacterial species and the unlike cell structures of the tested microorganisms, where unlike Gram-positive *S. aureus* bacteria, Gram-negative *E. coli* bacteria possess an outer membrane and a thick cell wall that result in a rigid outer coating **(Qiao et al., 2018)**.

4. Conclusion

In summary, divalent metal release out of pristine LDHs in broth culture media is strongly dependent on their physicochemical properties as their crystallinity, M^{II}:Al^{III} ratio, type of intercalated anion and nature of M^{II} cations. Lower crystallinity Zn_2Al:CO_3 LDH unexposed to hydrothermal treatment showed more defects and small aggregated particles and thus released more zinc ions in broth media. Increasing M^{II}:Al^{III} ratio in Zn^{II}-based LDH had also led an enhanced release of Zn^{II} ions probably due to the increase of amount of zinc initially present in the LDH structure and/or due to the reduction in crystallinity. Moreover, the crystallinity and structure of the powders were also influenced by the anionic exchange reactions which aimed at eliminating carbonate anions and exchanging them with other intercalating anions, thus resulting in an amplified release of ions as well. On the other hand, the dissolution properties of M^{II}-Al^{III} LDHs having different constituent divalent metals (M^{II}) is related to the thermodynamic stability of their $M^{II}(OH)_2$ hydroxide counterparts, with the exception of Cu^{II}-based LDHs which released a higher amount of Cu^{II}, probably due to its very poor crystallinity and irregular structure presenting defects. Finally, the antibacterial activity of the synthesized pristine LDHs was determined, where only Zn^{II} and Cu^{II}-based LDHs were able to demonstrate an inhibitory effect against *E. coli* and *S. aureus*. The superior antimicrobial activity of Zn^{II}-based LDHs even at lower release profiles suggest that the antimicrobial effect of pristine LDHs is dependent on the

nature of constituent divalent metal on the first place. In addition, the minimum inhibitory concentration (MIC), required to inhibit the growth of *E. coli* and *S. aureus*, of Zn^{II}-based LDHs decreased with the increasing released Zn^{II} amount which was initially controlled by the different studied physicochemical parameters, *e.g.* crystallinity of the LDHs, Zn^{II}:Al^{III} molar ratio and nature of intercalated anion. This provides an evidence about the tight relationship between divalent metal release out of LDHs and their antimicrobial activity behavior, thus supporting and validating the suggested mechanism for the antibacterial effect of pristine LDHs by metallic ions release. Divalent metal species could be leached out of the LDH, *e.g.*, Zn^{II} and Cu^{II} in this case, and then might interact in a way or another with the bacterial cell wall or bacterial compositional DNA to inhibit their growth. Therefore, by controlling the nature of constituent divalent metal and the different physicochemical parameters responsible for divalent metal release, pristine LDHs could serve as potential candidates in several antibacterial applications as antimicrobial coatings, *e.g.* dressing for protecting wounds, medical tools, protection against biocorrosion and cement additives.

Acknowledgment

We would like to acknowledge the spectroscopy and microscopy Service Facility of SMI LCPME (Université de Lorraine-CNRS– http://www.lcpme.cnrs-nancy.fr). Claire Genois from LCPME (Université de Lorraine-CNRS– http://www.lcpme.cnrs-nancy.fr) is particularly acknowledged for the ICP-MS analysis. We would also like to thank the plateforme PMD²X de l'Institut Jean Barriol de l'Université de Lorraine , in particular Pierrick Durand for the PXRD analysis. We thank Celine Caillet and Audrey Beaussart from the Pôle de compétences Physico-

Chimie de l'Environnement and the PhySI research team of LIEC (Université de Lorraine-CNRS, http://liec.univ-lorraine.fr/) for their help in the PSD analyses.

Funding

Financial support was received from the French Ministry of Higher Education (MESR), the French National Scientific Centre (CNRS). Jazia Awassa acknowledges the French Ministry of Higher Education for PhD grant.

References

Ahmed, A. A. A., Talib, Z. A., & Hussein, M. Z. (2013). Influence of Metallic Molar Ratio on the Electron Spin Resonance and Thermal Diffusivity of Zn–Al Layered Double Hydroxide. *Journal of Nanomaterials*, *2013*, 1–9. https://doi.org/10.1155/2013/639354

Allada, R. k. (2002). Thermochemistry and Aqueous Solubilities of Hydrotalcite-Like Solids. *Science*, *296*(5568), 721–723. https://doi.org/10.1126/science.1069797

Allada, R. K., Pless, J. D., Nenoff, T. M., & Navrotsky, A. (2005). Thermochemistry of Hydrotalcite-like Phases Intercalated with CO_3^{2-}, NO_3^-, Cl^-, I^-, and ReO_4^-. *Chemistry of Materials*, *17*(9), 2455–2459. https://doi.org/10.1021/cm047813x

Baek, M., Kim, I.-S., Yu, J., Chung, H. E., Choy, J.-H., & Choi, S.-J. (2011). Effect of Different Forms of Anionic Nanoclays on Cytotoxicity. *Journal of Nanoscience and Nanotechnology*, *11*(2), 1803–1806. https://doi.org/10.1166/jnn.2011.3408

Bélteky, P., Rónavári, A., Igaz, N., Szerencsés, B., Tóth, I. Y., Pfeiffer, I., Kiricsi, M., & Kónya, Z. (2019). Silver nanoparticles: Aggregation behavior in biorelevant conditions and its impact on biological activity. *International Journal of Nanomedicine, Volume 14*, 667–687. https://doi.org/10.2147/IJN.S185965

Benito, P., Labajos, F. M., & Rives, V. (2006). Microwave-treated layered double hydroxides containing Ni2+ and Al3+: The effect of added Zn2+. *Journal of Solid State Chemistry*, *179*(12), 3784–3797. https://doi.org/10.1016/j.jssc.2006.08.010

Bi, X., Zhang, H., & Dou, L. (2014). Layered Double Hydroxide-Based Nanocarriers for Drug Delivery. *Pharmaceutics*, *6*(2), 298–332. https://doi.org/10.3390/pharmaceutics6020298

Bini, M., & Monteforte, F. (2018). Layered Double Hydroxides (LDHs): Versatile and Powerful Hosts for Different Applications. *Journal of Analytical & Pharmaceutical Research*, *7*(1). https://doi.org/10.15406/japlr.2018.07.00206

Blais, J. F., Djedidi, Z., Cheikh, R. B., Tyagi, R. D., & Mercier, G. (2008). Metals Precipitation from Effluents: Review. *Practice Periodical of Hazardous, Toxic, and Radioactive Waste Management*, *12*(3), 135–149. https://doi.org/10.1061/(ASCE)1090-025X(2008)12:3(135)

Boclair, J. W., & Braterman, P. S. (1999). Layered Double Hydroxide Stability. 1. Relative Stabilities of Layered Double Hydroxides and Their Simple Counterparts. *Chemistry of Materials*, *11*(2), 298–302. https://doi.org/10.1021/cm980523u

Bontchev, R. P., Liu, S., Krumhansl, J. L., Voigt, J., & Nenoff, T. M. (2003). Synthesis, Characterization, and Ion Exchange Properties of Hydrotalcite $Mg_6Al_2(OH)_{16}(A)_x(A')_{2-x}\cdot 4H_2O$ (A, A' = Cl^-, Br^-, I^-, and NO_3^-, $2 \geq x \geq 0$) Derivatives. *Chemistry of Materials*, *15*(19), 3669–3675. https://doi.org/10.1021/cm034231r

Borkow, G., & Gabbay, J. (2005). Copper as a Biocidal Tool. *Current Medicinal Chemistry*, *12*(18), 2163–2175. https://doi.org/10.2174/0929867054637617

776 Bruins, M. R., Kapil, S., & Oehme, F. W. (2000). Microbial Resistance to Metals in the
777 Environment. *Ecotoxicology and Environmental Safety*, *45*(3), 198–207.
778 https://doi.org/10.1006/eesa.1999.1860
779 Carja, G., Kameshima, Y., Nakajima, A., Dranca, C., & Okada, K. (2009). Nanosized silver–
780 anionic clay matrix as nanostructured ensembles with antimicrobial activity.
781 *International Journal of Antimicrobial Agents*, *34*(6), 534–539.
782 https://doi.org/10.1016/j.ijantimicag.2009.08.008
783 Cavani, F., Trifirò, F., & Vaccari, A. (1991). Hydrotalcite-type anionic clays: Preparation,
784 properties and applications. *Catalysis Today*, *11*(2), 173–301.
785 https://doi.org/10.1016/0920-5861(91)80068-K
786 Cheng, H.-M., Gao, X.-W., Zhang, K., Wang, X.-R., Zhou, W., Li, S.-J., Cao, X.-L., & Yan, D.-
787 P. (2019). A novel antimicrobial composite: ZnAl-hydrotalcite with *p* -hydroxybenzoic
788 acid intercalation and its possible application as a food packaging material. *New Journal*
789 *of Chemistry*, *43*(48), 19408–19414. https://doi.org/10.1039/C9NJ03943K
790 Clark, I., Gomes, R. L., Crawshaw, C., Neve, L., Lodge, R., Fay, M., Winkler, C., Hull, M., &
791 Lester, E. (2019). Continuous synthesis of $Zn_2Al–CO_3$ layered double hydroxides: A
792 comparison of bench, pilot and industrial scale syntheses. *Reaction Chemistry &*
793 *Engineering*, *4*(4), 663–666. https://doi.org/10.1039/C8RE00241J
794 Crespo, I. (1997). Intercalation of iron hexacyano complexes in Zn,Al-hydrotalcite. *Solid State*
795 *Ionics*, *101–103*, 729–735. https://doi.org/10.1016/S0167-2738(97)00290-7
796 Cullity, B. D. (1978). *Elements of x-ray diffraction* (2d ed). Addison-Wesley Pub. Co.
797 Djebbi, M. A., Elabed, A., Bouaziz, Z., Sadiki, M., Elabed, S., Namour, P., Jaffrezic-Renault, N.,
798 & Amara, A. B. H. (2016). Delivery system for berberine chloride based on the

nanocarrier ZnAl-layered double hydroxide: Physicochemical characterization, release behavior and evaluation of anti-bacterial potential. *International Journal of Pharmaceutics*, *515*(1–2), 422–430. https://doi.org/10.1016/j.ijpharm.2016.09.089

Dutta, S., Jana, T. K., Halder, S. K., Maiti, R., Dutta, A., Kumar, A., & Chatterjee, K. (2020). Zn $_2$ Al- CO $_3$ Layered Double Hydroxide: Adsorption, Cytotoxicity and Antibacterial Performances. *ChemistrySelect*, *5*(20), 6162–6171. https://doi.org/10.1002/slct.202001264

El-Shahawy, A. A. G., Abo El-Ela, F. I., Mohamed, N. A., Eldine, Z. E., & El Rouby, W. M. A. (2018). Synthesis and evaluation of layered double hydroxide/doxycycline and cobalt ferrite/chitosan nanohybrid efficacy on gram positive and gram negative bacteria. *Materials Science and Engineering: C*, *91*, 361–371. https://doi.org/10.1016/j.msec.2018.05.042

Esteban-Tejeda, L., Palomares, F., Cabal, B., López-Píriz, R., Fernández, A., Sevillano, D., Alou, L., Torrecillas, R., & Moya, J. (2017). Effect of the Medium Composition on the Zn2+ Lixiviation and the Antifouling Properties of a Glass with a High ZnO Content. *Materials*, *10*(2), 167. https://doi.org/10.3390/ma10020167

Forano, C., Bruna, F., Mousty, C., & Prevot, V. (2018). Interactions between Biological Cells and Layered Double Hydroxides: Towards Functional Materials. *The Chemical Record*, *18*(7–8), 1150–1166. https://doi.org/10.1002/tcr.201700102

Galvão, T. L. P., Neves, C. S., Caetano, A. P. F., Maia, F., Mata, D., Malheiro, E., Ferreira, M. J., Bastos, A. C., Salak, A. N., Gomes, J. R. B., Tedim, J., & Ferreira, M. G. S. (2016). Control of crystallite and particle size in the synthesis of layered double hydroxides:

Macromolecular insights and a complementary modeling tool. *Journal of Colloid and Interface Science*, *468*, 86–94. https://doi.org/10.1016/j.jcis.2016.01.038

Herrero, M., Labajos, F., & Rives, V. (2008). Size control and optimisation of intercalated layered double hydroxides. *Applied Clay Science*, S0169131708001336. https://doi.org/10.1016/j.clay.2008.06.011

Hibino, T. (2014). Acid Treatment of Layered Double Hydroxides Containing Carbonate: Acid Treatment of Layered Double Hydroxides Containing Carbonate. *European Journal of Inorganic Chemistry*, *2014*(31), 5311–5321. https://doi.org/10.1002/ejic.201402372

Inmauddin (Ed.). (2019). Layered double Hydroxide Based Biosensors. In *Materials Research Foundations* (1st ed., Vol. 47, pp. 131–156). Materials Research Forum LLC. https://doi.org/10.21741/9781644900130-4

Iyi, N., Yamada, H., & Sasaki, T. (2011). Deintercalation of carbonate ions from carbonate-type layered double hydroxides (LDHs) using acid–alcohol mixed solutions. *Applied Clay Science*, *54*(2), 132–137. https://doi.org/10.1016/j.clay.2011.07.017

Jobbágy, M., & Regazzoni, A. E. (2011). Dissolution of nano-size Mg–Al–Cl hydrotalcite in aqueous media. *Applied Clay Science*, *51*(3), 366–369. https://doi.org/10.1016/j.clay.2010.11.027

Johnston, A.-L., Lester, E., Williams, O., & Gomes, R. L. (2021). Understanding Layered Double Hydroxide properties as sorbent materials for removing organic pollutants from environmental waters. *Journal of Environmental Chemical Engineering*, *9*(4), 105197. https://doi.org/10.1016/j.jece.2021.105197

Kamal, W., El Rouby, W. M. A., El-Gendy, A. O., & Farghali, A. A. (2018). Bimodal applications of LDH-chitosan nanocomposite: Water treatment and antimicrobial activity.

IOP Conference Series: Materials Science and Engineering, *464*, 012005. https://doi.org/10.1088/1757-899X/464/1/012005

Kannan, S., Rives, V., & Knözinger, H. (2004). High-temperature transformations of Cu-rich hydrotalcites. *Journal of Solid State Chemistry*, *177*(1), 319–331. https://doi.org/10.1016/j.jssc.2003.08.023

Kim, S., Fahel, J., Durand, P., André, E., & Carteret, C. (2017). Ternary Layered Double Hydroxides (LDHs) Based on Co-, Cu-Substituted ZnAl for the Design of Efficient Photocatalysts: Ternary Layered Double Hydroxides (LDHs) Based on Co-, Cu-Substituted ZnAl for the Design of Efficient Photocatalysts. *European Journal of Inorganic Chemistry*, *2017*(3), 669–678. https://doi.org/10.1002/ejic.201601213

Kloprogge, J. T., Wharton, D., Hickey, L., & Frost, R. L. (2002). Infrared and Raman study of interlayer anions CO_3^{2-}, NO_3^-, SO_4^{2-} and ClO_4^- in Mg/Al-hydrotalcite. *American Mineralogist*, *87*(5–6), 623–629. https://doi.org/10.2138/am-2002-5-604

Kovanda, F., Rojka, T., Bezdička, P., Jirátová, K., Obalová, L., Pacultová, K., Bastl, Z., & Grygar, T. (2009). Effect of hydrothermal treatment on properties of Ni–Al layered double hydroxides and related mixed oxides. *Journal of Solid State Chemistry*, *182*(1), 27–36. https://doi.org/10.1016/j.jssc.2008.09.014

Lee, J.-Y., Gwak, G.-H., Kim, H.-M., Kim, T., Lee, G. J., & Oh, J.-M. (2016). Synthesis of hydrotalcite type layered double hydroxide with various Mg/Al ratio and surface charge under controlled reaction condition. *Applied Clay Science*, *134*, 44–49. https://doi.org/10.1016/j.clay.2016.03.029

León-Vallejo, A. M., Velázquez-Herrera, F. D., Sampieri, Á., Landeta-Cortés, G., & Fetter, G. (2019). Study of layered double hydroxides as bactericidal materials against

Corynebacterium ammoniagenes, a bacterium responsible for producing bad odors from human urine and skin infections. *Applied Clay Science*, *180*, 105194. https://doi.org/10.1016/j.clay.2019.105194

Li, J., Zhang, S., Chen, Y., Liu, T., Liu, C., Zhang, X., Yi, M., Chu, Z., & Han, X. (2017). A novel three-dimensional hierarchical CuAl layered double hydroxide with excellent catalytic activity for degradation of methyl orange. *RSC Advances*, *7*(46), 29051–29057. https://doi.org/10.1039/C7RA03848H

Li, M., Li, L., & Lin, S. (2020). Efficient antimicrobial properties of layered double hydroxide assembled with transition metals via a facile preparation method. *Chinese Chemical Letters*, *31*(6), 1511–1515. https://doi.org/10.1016/j.cclet.2019.09.047

Li, M., Xu, Z. P., Sultanbawa, Y., Chen, W., Liu, J., & Qian, G. (2019). Potent and durable antibacterial activity of ZnO-dotted nanohybrids hydrothermally derived from ZnAl-layered double hydroxides. *Colloids and Surfaces B: Biointerfaces*, *181*, 585–592. https://doi.org/10.1016/j.colsurfb.2019.06.013

Li, M., Zhu, L., & Lin, D. (2011). Toxicity of ZnO Nanoparticles to *Escherichia coli*: Mechanism and the Influence of Medium Components. *Environmental Science & Technology*, *45*(5), 1977–1983. https://doi.org/10.1021/es102624t

Lieth, R. M. A. (Ed.). (1977). *Preparation and Crystal Growth of Materials with Layered Structures*. Springer Netherlands. https://doi.org/10.1007/978-94-017-2750-1

Liu, H., Jiao, Q., Zhao, Y., Li, H., Sun, C., & Li, X. (2010). Mixed oxides derived from Cu–Co layered double hydroxide nanorods: Preparation, characterization and their catalytic activities. *Journal of Alloys and Compounds*, *496*(1–2), 317–323. https://doi.org/10.1016/j.jallcom.2010.02.004

Liu, S., Killen, E., Lim, M., Gunawan, C., & Amal, R. (2014). The effect of common bacterial growth media on zinc oxide thin films: Identification of reaction products and implications for the toxicology of ZnO. *RSC Adv.*, *4*(9), 4363–4370. https://doi.org/10.1039/C3RA46177G

Liu, Y., & Yang, Z. (2016). Intercalation of sulfate anions into a Zn–Al layered double hydroxide: Their synthesis and application in Zn–Ni secondary batteries. *RSC Advances*, *6*(73), 68584–68591. https://doi.org/10.1039/C6RA09096F

Lobo-Sánchez, M., Nájera-Meléndez, G., Luna, G., Segura-Pérez, V., Rivera, J. A., & Fetter, G. (2018). ZnAl layered double hydroxides impregnated with eucalyptus oil as efficient hybrid materials against multi-resistant bacteria. *Applied Clay Science*, *153*, 61–69. https://doi.org/10.1016/j.clay.2017.11.017

Mahjoubi, F. Z., Khalidi, A., Abdennouri, M., & Barka, N. (2017). Zn–Al layered double hydroxides intercalated with carbonate, nitrate, chloride and sulphate ions: Synthesis, characterisation and dye removal properties. *Journal of Taibah University for Science*, *11*(1), 90–100. https://doi.org/10.1016/j.jtusci.2015.10.007

Mallakpour, S., Radfar, Z., & Hussain, C. M. (2021). Current advances on polymer-layered double hydroxides/metal oxides nanocomposites and bionanocomposites: Fabrications and applications in the textile industry and nanofibers. *Applied Clay Science*, *206*, 106054. https://doi.org/10.1016/j.clay.2021.106054

Mao, L., Liu, J., Zheng, S., Wu, H., Liu, Y., Li, Z., & Bai, Y. (2019). Mussel-inspired nano-silver loaded layered double hydroxides embedded into a biodegradable polymer matrix for enhanced mechanical and gas barrier properties. *RSC Advances*, *9*(10), 5834–5843. https://doi.org/10.1039/C8RA09602C

Marcato, P. D., Parizotto, N. V., Martinez, D. S. T., Paula, A. J., Ferreira, I. R., Melo, P. S., Durán, N., & Alves, O. L. (2013). New Hybrid Material Based on Layered Double Hydroxides and Biogenic Silver Nanoparticles: Antimicrobial Activity and Cytotoxic Effect. *Journal of the Brazilian Chemical Society*, *24*(2), 266–272. https://doi.org/10.5935/0103-5053.20130034

Mishra, G., Dash, B., Pandey, S., & Mohanty, P. P. (2013). Antibacterial actions of silver nanoparticles incorporated Zn–Al layered double hydroxide and its spinel. *Journal of Environmental Chemical Engineering*, *1*(4), 1124–1130. https://doi.org/10.1016/j.jece.2013.08.031

Mishra, G., Dash, B., Pandey, S., & Sethi, D. (2018). Ternary layered double hydroxides (LDH) based on Cu- substituted Zn Al for the design of efficient antibacterial ceramics. *Applied Clay Science*, *165*, 214–222. https://doi.org/10.1016/j.clay.2018.08.021

Mittapally, S., Taranum, R., & Parveen, S. (2018). Metal ions as antibacterial agents. *Journal of Drug Delivery and Therapeutics*, *8*(6-s), 411–419. https://doi.org/10.22270/jddt.v8i6-s.2063

Miyata, S. (1980). Physico-Chemical Properties of Synthetic Hydrotalcites in Relation to Composition. *Clays and Clay Minerals*, *28*(1), 50–56. https://doi.org/10.1346/CCMN.1980.0280107

Moaty, S. A. A., Farghali, A. A., & Khaled, R. (2016). Preparation, characterization and antimicrobial applications of Zn-Fe LDH against MRSA. *Materials Science and Engineering: C*, *68*, 184–193. https://doi.org/10.1016/j.msec.2016.05.110

Pasquet, J., Chevalier, Y., Pelletier, J., Couval, E., Bouvier, D., & Bolzinger, M.-A. (2014). The contribution of zinc ions to the antimicrobial activity of zinc oxide. *Colloids and Surfaces*

A: Physicochemical and Engineering Aspects, *457*, 263–274. https://doi.org/10.1016/j.colsurfa.2014.05.057

Pavlovic, M. (2016). Ion specific effects on the stability of layered double hydroxide colloids. *Soft Matter*, 10.

Peng, F., Wang, D., Zhang, D., Cao, H., & Liu, X. (2018). The prospect of layered double hydroxide as bone implants: A study of mechanical properties, cytocompatibility and antibacterial activity. *Applied Clay Science*, *165*, 179–187. https://doi.org/10.1016/j.clay.2018.08.020

Prasanna, S. V., & Kamath, P. V. (2009). Anion-Exchange Reactions of Layered Double Hydroxides: Interplay between Coulombic and H-Bonding Interactions. *Industrial & Engineering Chemistry Research*, *48*(13), 6315–6320. https://doi.org/10.1021/ie9004332

Qiao, Y., Li, Q., Chi, H., Li, M., Lv, Y., Feng, S., Zhu, R., & Li, K. (2018). Methyl blue adsorption properties and bacteriostatic activities of Mg-Al layer oxides via a facile preparation method. *Applied Clay Science*, *163*, 119–128. https://doi.org/10.1016/j.clay.2018.07.018

Radha, A. V., Vishnu Kamath, P., & Shivakumara, C. (2005). Mechanism of the anion exchange reactions of the layered double hydroxides (LDHs) of Ca and Mg with Al. *Solid State Sciences*, *7*(10), 1180–1187. https://doi.org/10.1016/j.solidstatesciences.2005.05.004

Rasouli, N., Movahedi, M., & Doudi, M. (2017). Synthesis and characterization of inorganic mixed metal oxide nanoparticles derived from Zn–Al layered double hydroxide and their antibacterial activity. *Surfaces and Interfaces*, *6*, 110–115. https://doi.org/10.1016/j.surfin.2016.11.007

Rawle, A. (2003). The Basic Principles of Particle Size Analysis. *Surface Coatings International Part A: Coatings Journal*, *86*, 58–65.

Rives, V. (Ed.). (2001). *Layered double hydroxides: Present and future*. Nova Science Publishers.

Rocha Oliveira, G., Dias do Amaral, L. J., Giovanela, M., da Silva Crespo, J., Fetter, G., Rivera, J. A., Sampieri, A., & Bosch, P. (2015). Bactericidal Performance of Chlorophyllin-Copper Hydrotalcite Compounds. *Water, Air, & Soil Pollution*, *226*(9), 316. https://doi.org/10.1007/s11270-015-2585-1

Rojas, R. (2016). Effect of particle size on copper removal by layered double hydroxides. *Chemical Engineering Journal*, *303*, 331–337. https://doi.org/10.1016/j.cej.2016.06.007

Salak, A. N., Tedim, J., Kuznetsova, A. I., Zheludkevich, M. L., & Ferreira, M. G. S. (2010). Anion exchange in Zn–Al layered double hydroxides: In situ X-ray diffraction study. *Chemical Physics Letters*, *495*(1–3), 73–76. https://doi.org/10.1016/j.cplett.2010.06.041

Salguero, Y., Valenti, L., Rojas, R., & García, M. C. (2020). Ciprofloxacin-intercalated layered double hydroxide-in-hybrid films as composite dressings for controlled antimicrobial topical delivery. *Materials Science and Engineering: C*, *111*, 110859. https://doi.org/10.1016/j.msec.2020.110859

Scarpellini, D., Falconi, C., Gaudio, P., Mattoccia, A., Medaglia, P. G., Orsini, A., Pizzoferrato, R., & Richetta, M. (2014). Morphology of Zn/Al layered double hydroxide nanosheets grown onto aluminum thin films. *Microelectronic Engineering*, *126*, 129–133. https://doi.org/10.1016/j.mee.2014.07.007

Sharma, M., & Prasher, P. (2020). Metallic Nanoparticles at the Biointerface. In C. Bhargava & A. Sachdeva (Eds.), *Nanotechnology* (1st ed., pp. 261–276). CRC Press. https://doi.org/10.1201/9781003082859-15

Sun, X., & Dey, S. K. (2015). Insights into the synthesis of layered double hydroxide (LDH) nanoparticles: Part 2. Formation mechanisms of LDH. *Journal of Colloid and Interface Science*, *458*, 160–168. https://doi.org/10.1016/j.jcis.2015.06.025

Tabti, H. A., Adjdir, M., Ammam, A., Mdjahed, B., Guezzen, B., Ramdani, A., Benddedouche, C. K., Bouchikhi, N., & Chami, N. (2020). Facile synthesis of Cu-LDH with different Cu/Al molar ratios: Application as antibacterial inhibitors. *Research on Chemical Intermediates*, *46*(12), 5377–5390. https://doi.org/10.1007/s11164-020-04268-8

Tammaro, L., Vittoria, V., & Bugatti, V. (2014). Dispersion of modified layered double hydroxides in Poly(ethylene terephthalate) by High Energy Ball Milling for food packaging applications. *European Polymer Journal*, *52*, 172–180. https://doi.org/10.1016/j.eurpolymj.2014.01.001

Theiss, F. L., Ayoko, G. A., & Frost, R. L. (2016). Synthesis of layered double hydroxides containing Mg2+, Zn2+, Ca2+ and Al3+ layer cations by co-precipitation methods—A review. *Applied Surface Science*, *383*, 200–213. https://doi.org/10.1016/j.apsusc.2016.04.150

Wang, C.-C., & Ying, J. Y. (1999). Sol−Gel Synthesis and Hydrothermal Processing of Anatase and Rutile Titania Nanocrystals. *Chemistry of Materials*, *11*(11), 3113–3120. https://doi.org/10.1021/cm990180f

Wang, L., Zhu, Z., Wang, F., Qi, Y., Zhang, W., & Wang, C. (2021). State-of-the-art and prospects of Zn-containing layered double hydroxides (Zn-LDH)-based materials for

photocatalytic water remediation. *Chemosphere*, *278*, 130367. https://doi.org/10.1016/j.chemosphere.2021.130367

Wang, Y., & Zhang, D. (2012). Synthesis, characterization, and controlled release antibacterial behavior of antibiotic intercalated Mg–Al layered double hydroxides. *Materials Research Bulletin*, *47*(11), 3185–3194. https://doi.org/10.1016/j.materresbull.2012.08.029

Wang, Z., Yu, H., Ma, K., Chen, Y., Zhang, X., Wang, T., Li, S., Zhu, X., & Wang, X. (2018). Flower-like Surface of Three-Metal-Component Layered Double Hydroxide Composites for Improved Antibacterial Activity of Lysozyme. *Bioconjugate Chemistry*, *29*(6), 2090–2099. https://doi.org/10.1021/acs.bioconjchem.8b00305

WHO. (2019). *New report calls for urgent action to avert antimicrobial resistance crisis*. World Health Organization. https://www.who.int/news/item/29-04-2019-new-report-calls-for-urgent-action-to-avert-antimicrobial-resistance-crisis

Williams, O., Clark, I., Gomes, R. L., Perehinec, T., Hobman, J. L., Stekel, D. J., Hyde, R., Dodds, C., & Lester, E. (2019). Removal of copper from cattle footbath wastewater with layered double hydroxide adsorbents as a route to antimicrobial resistance mitigation on dairy farms. *Science of The Total Environment*, *655*, 1139–1149. https://doi.org/10.1016/j.scitotenv.2018.11.330

Yang, Z., Zhang, C., Zeng, G., Tan, X., Huang, D., Zhou, J., Fang, Q., Yang, K., Wang, H., Wei, J., & Nie, K. (2021). State-of-the-art progress in the rational design of layered double hydroxide based photocatalysts for photocatalytic and photoelectrochemical H2/O2 production. *Coordination Chemistry Reviews*, *446*, 214103. https://doi.org/10.1016/j.ccr.2021.214103

Zhang, J., Zhang, F., Ren, L., Evans, D. G., & Duan, X. (2004). Synthesis of layered double hydroxide anionic clays intercalated by carboxylate anions. *Materials Chemistry and Physics*, *85*(1), 207–214. https://doi.org/10.1016/j.matchemphys.2004.01.020

Zhang, W., Zhao, Y., Wang, W., Peng, J., Li, Y., Shangguan, Y., Ouyang, G., Xu, M., Wang, S., Wei, J., Wei, H., Li, W., & Yang, Z. (2020). Colloidal Surface Engineering: Growth of Layered Double Hydroxides with Intrinsic Oxidase- Mimicking Activities to Fight Against Bacterial Infection in Wound Healing. *Advanced Healthcare Materials*, *9*(17), 2000092. https://doi.org/10.1002/adhm.202000092

Zheng, Q., Hao, Y., Ye, P., Guo, L., Wu, H., Guo, Q., Jiang, J., Fu, F., & Chen, G. (2013). A pH-responsive controlled release system using layered double hydroxide (LDH)-capped mesoporous silica nanoparticles. *Journal of Materials Chemistry B*, *1*(11), 1644. https://doi.org/10.1039/c3tb00518f

Figures:

Supplementary Material

Divalent Metal Release and Antimicrobial Effects of Layered Double Hydroxides

Jazia Awassa[1], Damien Cornu[1], Samantha Soulé[1], Cédric Carteret[1], Christian Ruby[1]*, Sofiane El-Kirat-Chatel[1]

[1]Laboratoire de Chimie Physique et Microbiologie pour les Matériaux et l'Environnement (LCPME), Université de Lorraine, 405 Rue de Vandoeuvre, 54600, Villers-lès-Nancy, France

Table S1. Experimental conditions for the synthesis of carbonated LDHs.

LDH sample	$M^{II}:Al^{III}$	$n(M^{II})$ (mol)	$n(M^{III})$ (mol)	Hydrothermal treatment	$M^{II}:Al^{III}$ determined by ICP
$Zn_2Al:CO_3$-hyd	2	0.053	0.027	Yes	1.9
$Zn_2Al:CO_3$-cop	2	0.053	0.027	No	1.9
$Zn_3Al:CO_3$	3	0.060	0.020	Yes	2.9
$Cu_2Al:CO_3$	2	0.053	0.027	Yes	2
$Ni_2Al:CO_3$	2	0.053	0.027	Yes	1.9
$Co_2Al:CO_3$	2	0.053	0.027	Yes	2
$Mg_2Al:CO_3$	2	0.053	0.027	Yes	2.1

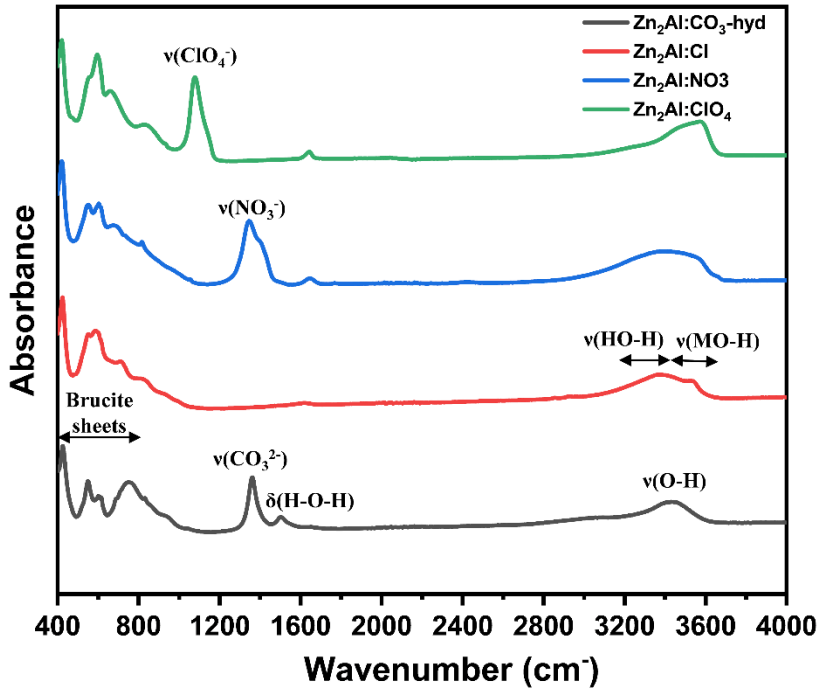

1068

1069 **Figure S1.** Infrared spectra (ATR) of Zn_2Al LDHs with different intercalating anions.

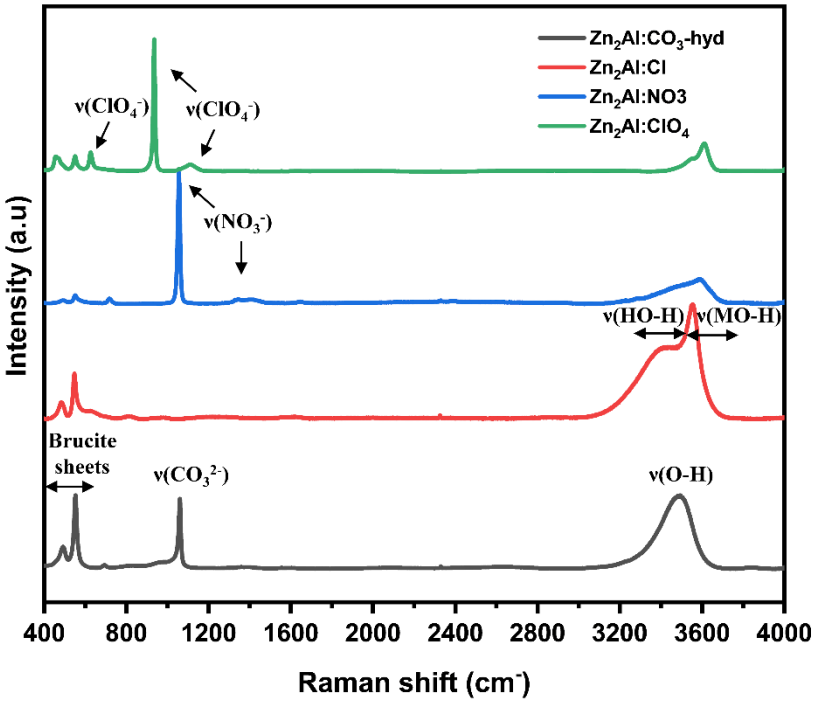

1070

1071 **Figure S2.** Raman spectra of Zn_2Al LDHs with different intercalating anions.

Table S2. Partial dissolution profiles of all synthesized LDH samples into M^{II} in in terms of average percentage compared to the initial amount present in the LDH.

LDH sample	Percentage of released M^{II} (%)
$Zn_2Al:CO_3$-hyd, $Zn_2Al:CO_3$-cop, $Zn_3Al:CO_3$, $Zn_2Al:Cl$, $Zn_2Al:NO_3$, $Zn_2Al:ClO_4$, $Cu_2Al:CO_3$, $Ni_2Al:CO_3$, $Co_2Al:CO_3$, $Mg_2Al:CO_3$	Below detection point

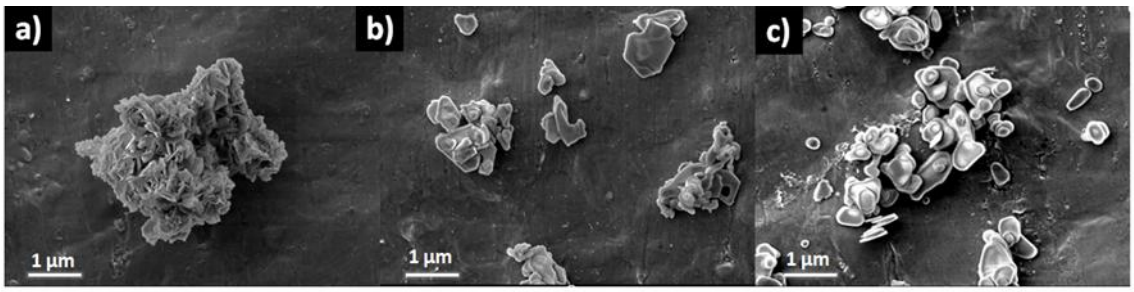

Figure S3. SEM micrographs of: a)$Zn_2Al:Cl$, b) $Zn_2Al:NO_3$, c) $Zn_2Al:ClO_4$.

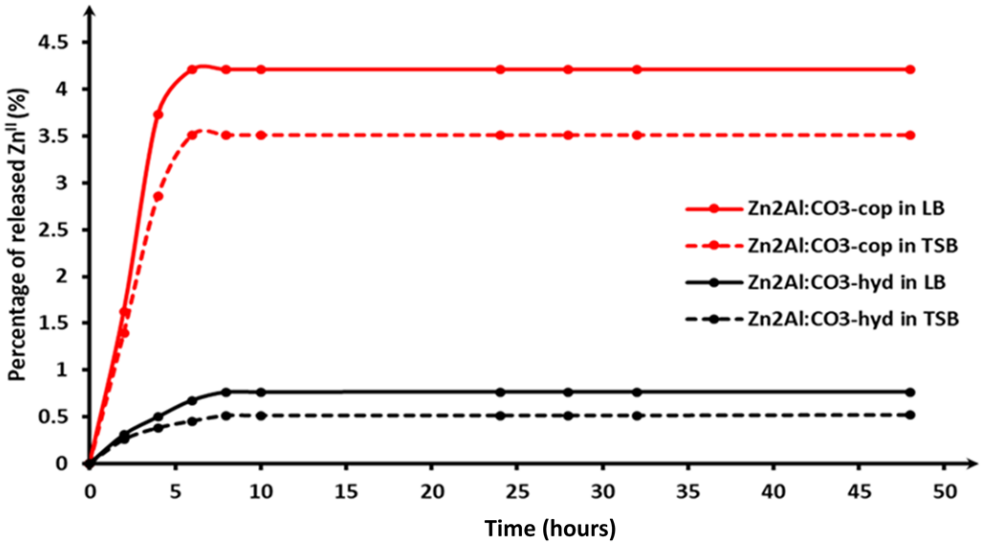

Figure S4. Dissolution profiles of $Zn_2Al:CO_3$-hyd and $Zn_2Al:CO_3$-cop over time.

Table S3. pKsp values for $M^{II}(OH)_2$ reported by **(Blais et al., 2008)**.

Metal hydroxide	pK_{sp}

$Zn^{II}(OH)_2$	15.7
$Cu^{II}(OH)_2$	18.6
$Ni^{II}(OH)_2$	14.7
$Co^{II}(OH)_2$	14.8
$Mg^{II}(OH)_2$	10.8

1080